Studies on Triplet Sensitization Processes for Photon Upconversion

奥村, 佳亮

https://doi.org/10.15017/4060108

出版情報：九州大学, 2019, 博士（工学）, 課程博士
バージョン：
権利関係：

Studies on Triplet Sensitization Processes for Photon Upconversion

Keisuke Okumura

Department of Chemistry and Biochemistry
Graduate School of Engineering
Kyushu University

March 2020

Table of Contents

Chapter 1. Introduction

1-1. Solar energy and photon upconversion

Reserves of fossil fuels on which humanity depends are declining rapidly, causing demand for alternative energy sources. Clean alternative energy supplies should emit no greenhouse gases, which cause global warming, climate change, and ocean acidification.

Solar energy has been widely harnessed as a clean, abundant and sustainable energy source. Vast quantities of energy are constantly released by the sun and power the oceanic and atmospheric currents on earth. The amount of energy consumed annually by humans, 4.6×10^{20} joules, is provided to earth by the sun in one hour.[1]

To utilize the energy in sunlight, many solar energy conversion systems have been developed, in which sunlight is converted into electricity, fuel, and heat. Solar energy conversion systems such as photovoltaics and photocatalysis, however, harness only a part of the overall solar energy. This is primarily because of the limited optical absorption of the light-harvesting materials used (Figure 1-1). If the photon energy is higher than the bandgap of the material, the excess energy is wasted in the production of heat by the thermalization of excited charge carriers. Photons with sub-bandgap energy are not harvested thoroughly.[2]

Photon upconversion (UC), the process of converting two or more photons into one higher-energy photon, has attracted interest for a broad range of applications. Firstly, UC is considered a promising method to improve solar energy conversion efficiencies in photovoltaic systems. Because amorphous silicon solar cells and perovskite solar cells are not sensitive to the infrared region, which contains almost half the energy in solar radiation, the upconversion of near-infrared (NIR) photons would contribute significantly to overcoming the Shockley-Queisser efficiency limit (33.7% for a single junction solar cell)[3] by harnessing a larger number of photons. Trupke *et al.* published the first theoretical study on upconversion-assisted solar cells based on detailed balance calculations. They showed that the upconversion of sub-bandgap photons improves the conversion efficiency in combination with ideal upconversion materials. The maximum energy conversion efficiency was calculated to be 47.6% under non-concentrated sunlight, assuming 6000 K thermal blackbody radiation.[4] While crystalline silicon solar cells can operate with NIR light, high cost and time-consuming production processes have limited their commercial use.

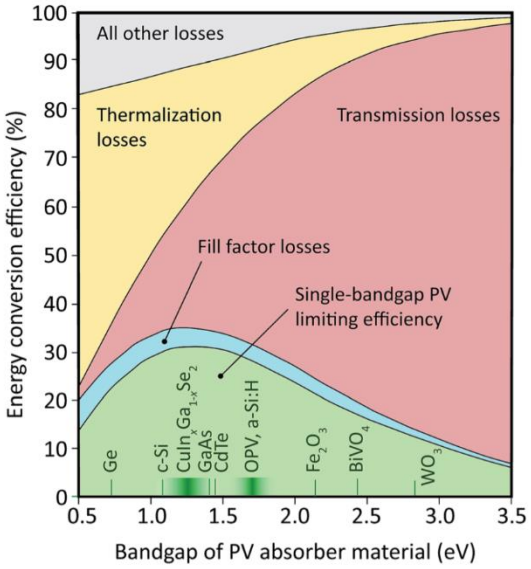

Figure 1-1. Relative importance of fundamental loss mechanisms in solar energy conversion as a function of photovoltaic absorber bandgap, with examples of absorber materials.[2]

The production of high-energy photons in the ultraviolet (UV) region from visible light by a UC system is particularly useful for photocatalysis applications because most current photocatalytic systems are driven only by UV light or high-energy visible light due to the bandgaps of the component materials. By taking advantage of high permeability of NIR light in living tissues, NIR-to-visible UC could be used for biological applications including photoinduced drug release, photodynamic therapy, and optogenetics.

1-2. Photon upconversion based on triplet-triplet annihilation (TTA-UC)

Of some UC mechanisms, triplet-triplet annihilation-based UC (TTA-UC) is particularly promising for a broad range of applications from energy to biology because it works with low-intensity, noncoherent incident light such as sunlight.[2, 5-16]

In a conventional TTA-UC system, excited triplet states of emitter molecules are populated by triplet energy transfer (TET) from molecular sensitizers with high intersystem crossing (ISC) efficiency. This is followed by annihilation between two triplets of the emitter, which produces a higher-energy excited singlet state of the emitter that results in the emission of upconverted delayed fluorescence (Figure 1-2).

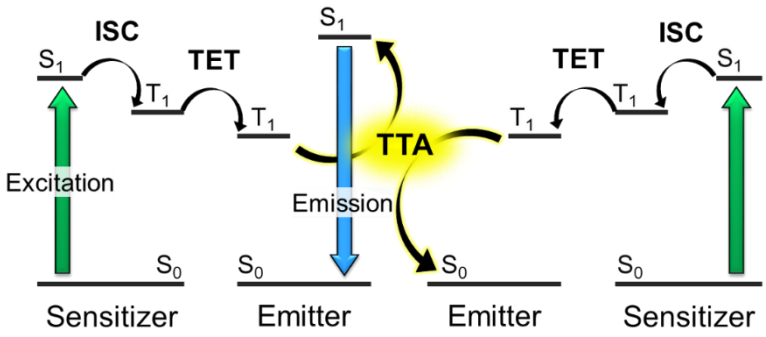

Figure 1-2. Scheme for the mechanism of conventional TTA-UC, showing the energy levels involved (S = singlet, T = triplet, ISC = intersystem crossing, TET = triplet energy transfer, TTA = triplet-triplet annihilation).

1-3. Current state of TTA-UC system

Until recently, many TTA-UC studies focused on finding sensitizer and emitter molecules for efficient TTA-UC, and various wavelength conversions have been reported with different sensitizer-emitter combinations (Figure 1-3, top).[17] Most TTA-UC studies, however, have been targeted at visible-to-visible UC, especially green-to-blue UC, for which platinum (II) octaethylporphyrin (PtOEP) sensitizer and 9,10-diphenylanthracene (DPA) emitter are a benchmark combination. Though there have been recent works on NIR-to-visible and visible-to-UV TTA-UC, they remain major challenges in TTA-UC research.

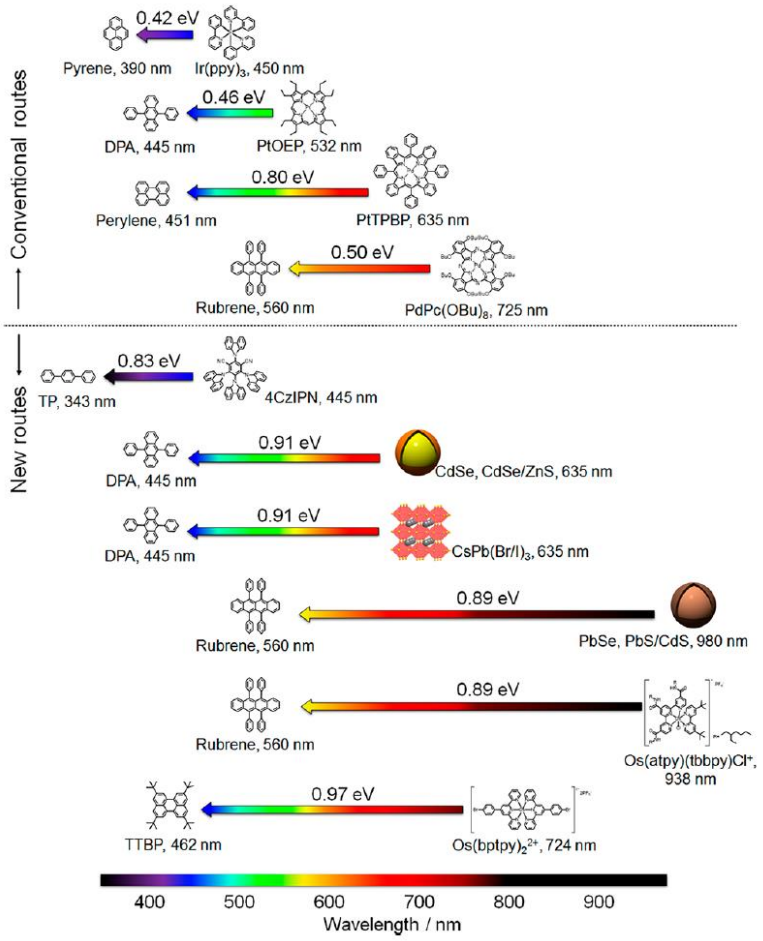

Figure 1-3. Representative combinations of sensitizer (right) and emitter (left) and their respective excitation and emission wavelengths. The widths of the anti-Stokes shift are also shown.[17]

Although conventional TTA-UC systems can work with low excitation intensity and give high UC efficiencies, there are some fundamental problems related to triplet sensitizers. Conventional sensitizer molecules harvest only a limited range of light because of their narrow absorption bands. Additionally, laborious molecular design and organic syntheses are required to obtain sensitizer molecules with appropriate photophysical properties. Large intrinsic energy losses in the triplet sensitization processes, namely ISC and TET, reduce the attainable anti-Stokes shifts. The anti-Stokes shift, defined as the energy difference between excited and emitted light, is an important parameter for UC systems. While other UC mechanisms based on multistep excitation or multiphoton absorption give large anti-Stokes shifts, their applications are limited because they usually require high-power excitation (W cm^{-2} ~ MW cm^{-2}).[18-20] By contrast, TTA-UC mechanism works with much lower excitation intensity (~ mW cm^{-2}) and has a wider range of potential applications.

1-4. New class of molecular sensitizers for extended anti-Stokes shifts

1-4-1. TADF molecules

New classes of triplet sensitizers can help achieve large anti-Stokes shifts in TTA-UC (Figure 1-3, bottom).[17] Several reports demonstrated molecules that exhibit thermally activated delayed fluorescence (TADF) can function as triplet sensitizers.[21-26] TADF molecules have remarkably small S_1-T_1 energy gaps, which circumvent the significant energy loss in the ISC process (Figure 1-4). The absence of heavy metals such as Pt or Pd is an added benefit in terms of toxicity and cost.

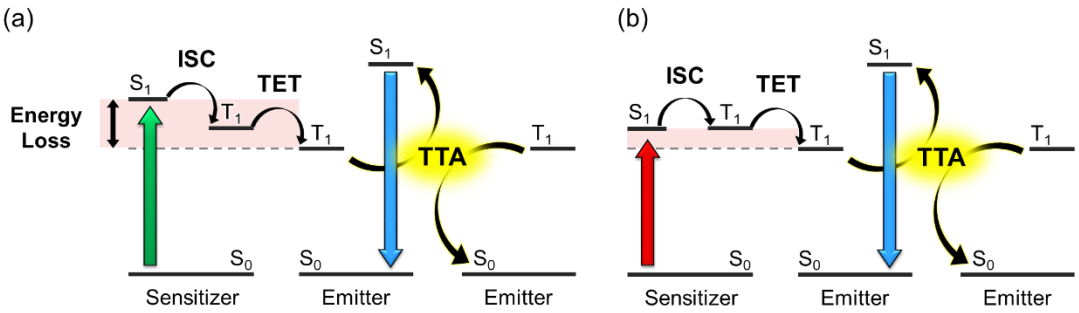

Figure 1-4. Schemes for the mechanism of (a) TTA-UC with conventional molecular sensitizers and (b) TTA-UC with TADF sensitizers.

The first example of a TADF molecule-sensitized TTA-UC system was reported by Wu and co-workers.[21] To sensitize DPA, they used a red TADF molecule, 2,3,5,6-tetrakis(3,6-diphenylcarbazol-9-yl)-1,4-dicyanobenzene (4CzTPN-Ph), developed by Adachi and co-workers.[27] The DPA/4CzTPN-Ph bilayer thin film showed upconverted emission from DPA under laser excitation at 532 nm. In this solid-state system, the overall UC efficiency was limited (0.28%) because of the low TET efficiency of 9.1%.

Peng *et al.* applied a bichromophoric strategy for a TADF sensitizer to enhance TET efficiency, in which 2,7-di-*tert*-butylpyrene (DBP) was covalently tethered to a TADF molecule, 3,4,5,6-tetrakis-(carbazol-9-yl)-1,2-dicyanobenzene (4CzPN).[22] Polyurethane films containing 4CzPN-*n*DBP sensitizers and DBP emitters showed more efficient visible (450 nm)-to-UV (378 nm) TTA-UC compared to the film of unmodified 4CzPN and DBP, thanks to the suppressed reverse ISC and TADF pathways.

By utilizing the full potential of a TADF sensitizer, Yanai *et al*. achieved TTA-UC with large anti-Stokes shifts.[23] They used a typical TADF molecule, 2,4,5,6-tetrakis(carbazol-9-yl)isophthalonitrile (4CzIPN), to sensitize a UV emitter, *p*-terphenyl (TP), with high triplet and single energy levels. A deaerated solution of 4CzIPN and TP in benzene exhibited efficient visible (445 nm)-to-UV (343 nm) TTA-UC with a large anti-Stokes shift of 0.83 eV.

Very recently, Chen *et al.* reported red (635 nm)-to-blue (428 nm) TTA-UC with a large anti-Stokes shift of 0.94 eV.[26] As a TADF sensitizer, they used a derivative of 2',7'-dichlorofluorescein (DCF) named DCF-MPYM, which absorbs in the red spectral region and has a long triplet state lifetime of 22 μs. Blue UC emission was clearly observed from a deaerated solution of DCF-MPYM and DPA in THF. The UC efficiency of 11.2% was substantially higher than that of other TADF molecule-sensitized TTA-UC systems.

1-4-2. Osmium complexes with S-T absorption

To avoid the energy loss inherent in the ISC process, a totally different strategy based on direct singlet-to-triplet (S-T) absorption has recently been proposed.[28-32] In this approach, an excited triplet state of the sensitizer is directly generated through S-T absorption, thus bypassing the S_1-to-T_1 ISC process. The absence of an ISC process decreases the energy loss in the triplet sensitization process, resulting in a larger anti-Stokes shift (Figure 1-5). Although direct S-T transition is generally considered to be a spin-forbidden process, it becomes weakly allowed in some metal complexes because of strong spin-orbit coupling, resulting in relatively large absorption coefficients.[33-37]

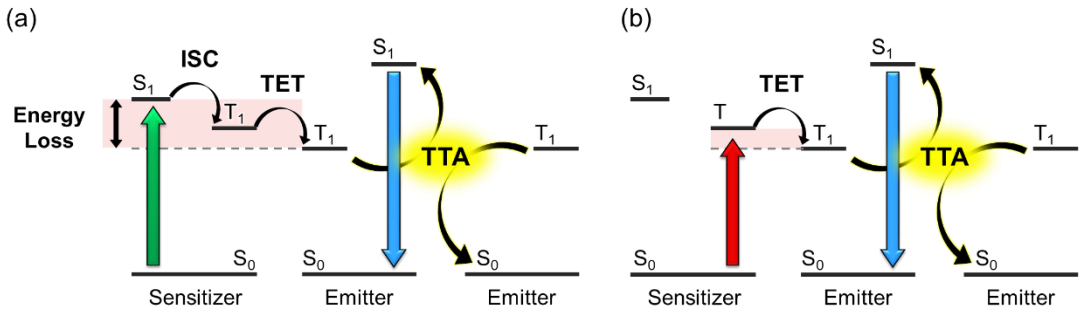

Figure 1-5. Schemes for the mechanism of (a) TTA-UC with conventional molecular sensitizers and (b) TTA-UC with S-T absorption sensitizers.

Amemori and Sasaki *et al.* used an osmium complex, Os(atpy)(tbbpy)Cl^+ (atpy = tris(2-ethylhexyl)-[2,2':6',2"-terpyridine]-4,4',4"-tricarboxamide; tbbpy = 4,4'-di-*tert*-butyl-2,2'-bipyridine) as a sensitizer with direct S-T absorption.[28] They observed NIR (938 nm)-to-yellow (570 nm) TTA-UC with an anti-Stokes shift of 0.86 eV in a dichloromethane solution containing the Os complex and rubrene. The TET process was found to be very inefficient in solution because of the short triplet lifetime of the Os complex (12 ns) caused by the large spin-orbit coupling. This problem was resolved by taking advantage of triplet energy migration-based UC in chromophore assemblies.[12, 13, 38-42] Nanoparticles of amorphous rubrene doped with the Os complex were prepared by re-precipitation and dispersed into poly(vinyl alcohol) (PVA) to prevent oxygen from quenching the triplet states. The resultant PVA film showed NIR-to-yellow TTA-UC with a high UC efficiency of 3.1% under aerated conditions. This indicates that TET from sensitizers to emitters is efficient because of the short distance between them.

Using the same approach with a different Os complex, Sasaki *et al.* demonstrated the first example of NIR (724 nm)-to-blue (462 nm) TTA-UC with a large anti-Stokes shift of 0.97 eV.[29] They carefully designed a sensitizer with S-T absorption, $Os(bptpy)_2^{2+}$ (bptpy = 4'-(4-bromophenyl)-2,2':6',2"-terpyridine) to have the appropriate triplet energy level for a blue-emitting molecule, 2,5,8,11-tetra-*tert*-butylperylene (TTBP). A deaerated solution of $Os(bptpy)_2^{2+}$ and TTBP in DMF showed NIR-to-blue TTA-UC with UC efficiency of 2.7%. In addition, solid-state NIR-to-blue TTA-UC was observed even under aerated conditions by encapsulating a ground solid mixture of $Os(bptpy)_2^{2+}$ and TTBP in a PVA matrix.

Sasaki *et al.* also reported the first example of optogenetics based on NIR-to-blue TTA-UC hydrogels utilizing an S-T absorber.[32] They developed a new complex, $Os(peptpy)_2^{2+}$, that has an interlinked structure of $Os(ptpy)_2$ (ptpy = 4'-phenyl-2,2':6',2"-terpyridine) units and phenyl-perylene units. The perylene moieties have a long-lived triplet state that results in energy-pooling by intramolecular energy transfer. This gives the sensitizer an exceptionally long excited-state lifetime, which is advantageous for TET, especially in viscous matrices such as hydrogels. In comparison with their previous system, higher UC efficiency of 5.9% was obtained from a deaerated solution of $Os(peptpy)_2^{2+}$ and TTBP in DMF.

Using the molecular sensitizers with S-T absorption are a promising method of sensitization for TTA-UC to reduce energy losses and achieve large anti-Stokes shifts. The direct population of excited triplets in emitter molecules by S-T absorption is also attractive because it can eliminate energy losses from both ISC and TET. While the S-T absorption of organic crystals has been studied in the field of triplet photophysics since the 1960s,[43-45] they have not been used as UC materials because S-T absorption is spin-forbidden. However, when the molecule is modified with heavy halogen atoms, S-T absorption becomes feasible because of strong spin-orbit coupling, and occurs at relatively low excitation intensity.[46] We exploited this behavior to demonstrate sensitizer-free TTA-UC in pure organic crystals (Chapter 4).

1-4-3. Other new molecular sensitizers

In addition to the two approaches described in the preceding section, some new approaches have been recently demonstrated to extend anti-Stokes shifts. Han *et al.* proposed a new triplet sensitization route, excited doublet-triplet energy transfer (DTET).[47] As a triplet sensitizer, they used a π-radical dye, (4-*N*-carbazolyl-2,6-dichlorophenyl)-bis(2,4,6-trichlorophenyl)-methyl (TTM-1Cz), with superior doublet emission. The excited doublet of TTM-1Cz was directly generated by photoexcitation, which was followed by direct sensitization of DPA through DTET. In this system, red (635 nm)-to-blue (432 nm) TTA-UC with a large anti-Stokes shift of 0.92 eV was achieved.

In another new strategy to increase anti-Stokes shifts in TTA-UC, Wang *et al.* focused on spin-allowed charge transfer absorption.[48] They used a covalently-linked BODIPY-perylene derivative that allowed spin-orbit charge transfer intersystem crossing (SOCT-ISC). The SOCT-ISC sensitizer creates a red-shifted charge transfer absorption band. Direct S_0-to-^{1}CT photoexcitation followed by ^{1}CT-to-T_1 ISC results in a smaller energy loss in the sensitization process than conventional routes. The triplet sensitization of perylene with the sensitizer led to red (589 nm)-to-blue (450 nm) TTA-UC with an anti-Stokes shift of 0.65 eV.

Fan *et al.* reported a chemical modification strategy to tune both the singlet and triplet excited-state energy levels of triplet sensitizers.[49] They precisely adjusted the excited energy levels of Pt-salophen complexes to minimize energy loss in the triplet sensitization of DPA by conjugation with each other or with an alternate chromophore via an ethynylene or butadiynylene bridge. The resulting Pt-salophen derivatives allowed red (635 nm)-to-blue (409 nm) TTA-UC with a large anti-Stokes shift of 1.08 eV.

Although successful examples are still limited, the development of new types of triplet sensitizer holds great promise for TTA-UC with the large anti-Stokes shifts required for practical applications.

1-5. Inorganic sensitizers

1-5-1. Metal chalcogenide quantum dots

Inorganic semiconductor materials have also been used as alternative triplet sensitizers to solve some of the problems of molecular triplet sensitizers. Metal chalcogenide quantum dots (QDs) have attracted particular attention. Quantum dots are quantum-confined semiconductor nanocrystals such as cadmium selenide (CdSe) and lead sulfide (PbS). Quantum confinement results in unique optoelectronic properties that differ substantially from the properties of bulk state. Potential applications include photovoltaics, light-emitting diodes, displays, lasers, transistors and biomedical imaging.

Quantum dots are excellent light absorbers with broad absorption properties. The bandgap of a QD is finely tunable by varying the particle size, and QDs have emissions with small Stokes shifts. These properties are entirely unlike those of common organometallic complexes. Quantum dots have a mixed-spin character because of the small exchange interaction and the strong spin-orbit coupling.[50, 51] This implies that energy transfer between QDs and molecular triplet states is spin-allowed.

In 2014, two research groups independently demonstrated that triplet excitons generated through singlet fission in organic semiconductor film can transfer the energy to inorganic semiconductor QDs.[52, 53] Tabachnyk *et al.* reported that interfacial energy transfer occurs from the excited triplets of pentacene to PbSe QDs in the bilayer sample.[52] They investigated the dynamics of triplet excitons by using ultrafast optical absorption spectroscopy. The photoexcitation of pentacene was followed by singlet fission to produce excited triplet states. Subsequently, the triplet was found to rapidly (<1 ps) transfer to QDs at the interface. They also revealed that the energy transfer occurs efficiently only when the QD bandgap is resonant with the triplet energy of pentacene (less than ±0.2 eV).

Thompson *et al.* demonstrated direct energy transfer from excited triplets of tetracene to PbS QDs in the bilayer sample.[53] After preferentially exciting tetracene, the singlet excitons in the thin tetracene film first underwent singlet fission. The triplets thus generated were transferred to the QDs. This energy transfer was confirmed by observing the appearance of tetracene peaks in the excitation spectrum of QD luminescence. They also found that the energy transfer efficiency had an exponential dependence on the lengths of the QD ligands, which is consistent with Dexter-type energy transfer.

Shortly after these results were published in 2014, at least four research groups including ours independently reported triplet energy transfer in the opposite direction (*i.e.*, from QDs to molecules) as a new triplet sensitization process.[54-57] Unlike conventional TTA-UC sensitized by molecular sensitizers, the energy losses in the triplet sensitization process are lower because of their single-triplet mixed-spin character, which enables TTA-UC with a large anti-Stokes shift (Figure 1-6).

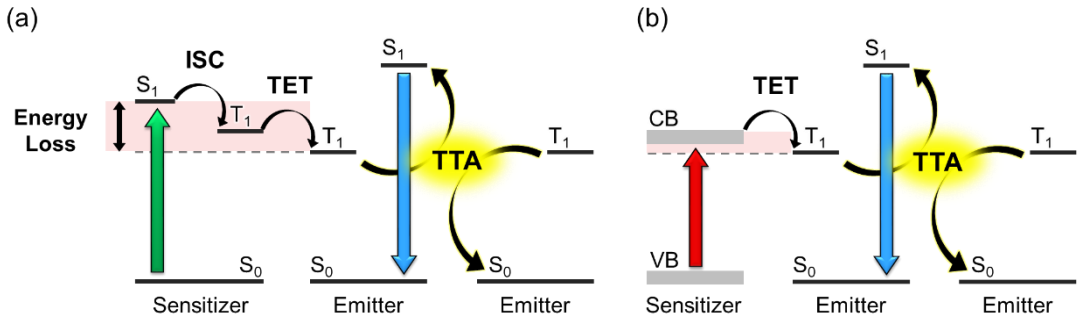

Figure 1-6. Schemes for the mechanism of (a) TTA-UC with molecular sensitizers and (b) TTA-UC with inorganic sensitizers (VB = valence band, CB = conduction band).

The first published example of triplet sensitization by QDs for TTA-UC was by Huang and co-workers (Figure 1-7a).[54] They demonstrated NIR (980 nm)-to-yellow (568 nm) TTA-UC in solution using PbSe QDs and rubrene as the sensitizer and emitter, respectively. The UC efficiency was measured to be 0.01%. They also observed green (532 nm)-to-blue (432 nm) TTA-UC with a higher UC efficiency of 9% in a solution with CdSe QDs/9-anthracenecarboxylic acid (ACA)/DPA as a sensitizer/ transmitter/emitter combination. The transmitter molecules anchored on the QD surface mediate TET between QDs and emitters to improve the efficiency. The transmitter molecules are discussed in detail later.

Wu *et al.* demonstrated solid-state NIR (>1 μm)-to-red (612 nm) TTA-UC that used PbS QDs and rubrene as the sensitizer and emitter, respectively (Figure 1-7b).[55] Upon photoexcitation of submonolayer PbS QDs, spin-triplet excitons were generated and transferred to the adjacent rubrene/ dibenzotetraphenylperiflanthene (DBP) layer, followed by TTA in rubrene and emission from DBP. Under laser excitation at λ = 808 nm, this solid-state material had a UC efficiency of 1.2%.

Mongin *et al.* experimentally provided proof-of-concept that triplet excitons can be extracted from QDs via interfacial Dexter-like energy transfer (Figure 1-7c).[56] Using transient absorption spectroscopy, they observed direct TET from CdSe QDs to surface-attached polyaromatic carboxylic acid acceptors, ACA and 1-pyrenecarboxylic acid (PCA). The experimental results also demonstrated the secondary TET process from surface-attached molecules to freely diffusing molecules with low-lying triplet levels.

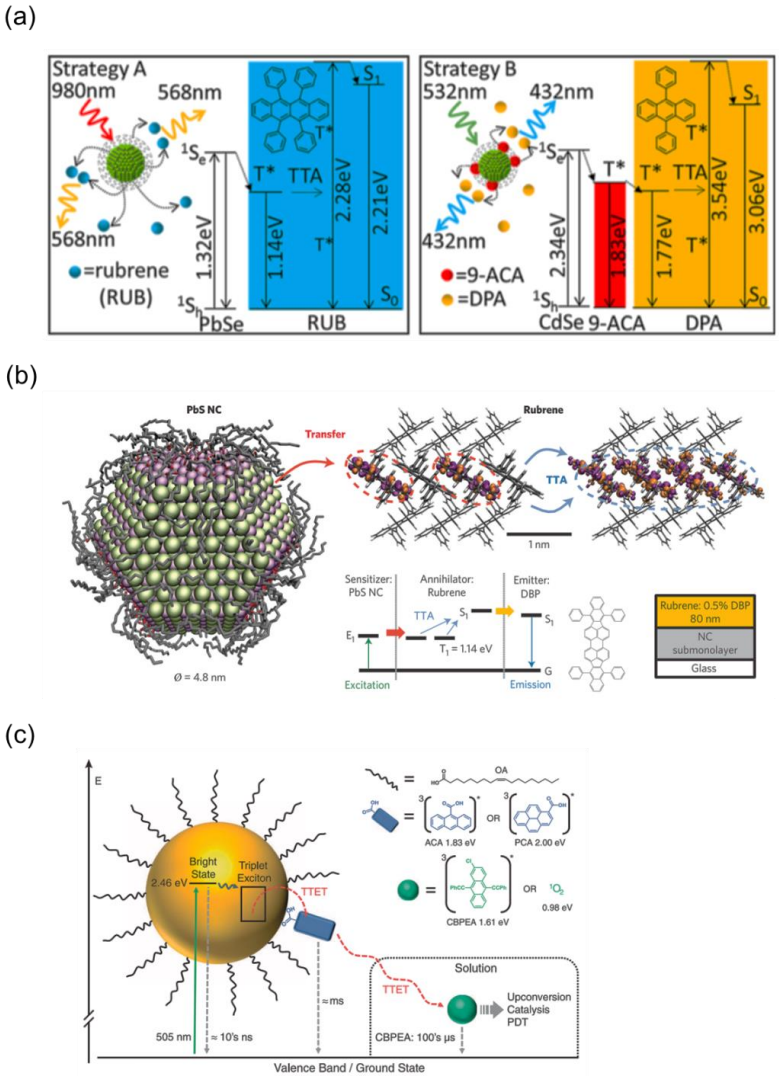

Figure 1-7. (a) Schematic illustrations and energy diagrams for TTA-UC system using PbSe/rubrene (left) and CdSe/ACA/DPA (right).[54] (b) Schematic illustration and energy diagram for TTA-UC system using PbS/rubrene/DBP, and the solid-state device structure.[55] (c) Schematic illustration of QD-to-solution triplet energy transfer, the associated energy levels, and the various TET and decay pathways investigated in the study.[56]

Around the same time, our work (described in Chapter 2) was conducted independently of these pioneering works.[57] Our research focused on core-shell CdSe/ZnS QDs, while other workers studied core-only QDs without shell layers. The photophysical properties of core-shell QDs are generally superior compared with core-only QDs because non-radiative recombination sites on the core surface are passivated by a wider bandgap semiconductor shell layer, which can improve TET efficiency.[58, 59] The core-shell structure is especially important when ligand exchange is performed because the process of ligand exchange can damage the surface and create trap states.[60]

Another means of promoting energy transfer is the modification of the QD surface with energy transmitter molecules. The surfaces of as-prepared QDs are usually capped by long-chain ligands such as oleic acid and octadecylamine, which are necessary to passivate dangling bonds for the suppression of non-radiative recombination and to increase solubility in various organic solvents.[59, 61] The mechanism of TET from QDs to organic molecules is of the Dexter-type, based on wave function overlap, and has an exponential dependence on the donor-acceptor distance. The long-chain ligands on the as-prepared QD surface spatially separate QDs from surrounding emitter molecules, which results in low TET efficiencies.[62] We modified the QD surface with energy transmitter molecules, and the short distance between the QDs and surface-attached transmitter ligands allowed for efficient Dexter energy transfer. It is expected that transmitter molecules mediate TET to free emitter molecules in bulk solution because triplet lifetimes becomes long enough on transmitter ligands to allow sufficient time for TET. Energy transmitters were also used in the work of Huang *et al.*, who used ACA.[54] Though the molecules including their metal-binding moieties were different, the results are consistent with each other.

The importance of both the core-shell structure of QDs and transmitter molecules for efficient triplet sensitization has been supported by the results of Tang and co-workers.[63-68] They studied PbS/CdS QDs,[63] CdS/ZnS QDs,[64] and CdSe/ZnS QDs,[65] and found that UC efficiency is strongly dependent on the thickness of the shell layer. The shell enhances TET by passivating the surface trap, but a thick shell acts as an energy barrier that diminishes TET. There is an optimal shell thickness at which the UC efficiency is maximized.

The surface density of transmitter ligands is one of the keys to facilitating TET. The efficiency of UC reaches a maximum and then decreases as the surface density of transmitter ligand increases.[66] Additional transmitter ligands can cause TTA between neighboring transmitters on the surface, lowering the efficiency of transmitter-to-emitter TET. The molecular design of the transmitter ligand is also important. Because orbital overlap is crucial for Dexter-type TET, the distance between the QD and chromophore (polyacene moiety),[67] and the binding geometry[68] greatly affect TET efficiency. In addition, the binding moiety (functional group) and consequent binding affinity are important because they impact the surface density of transmitter ligands and the stability of the QD-transmitter hybrid.[69] Recent advances described here provide strategic insight into the optimal design of hybrid interfaces for QD-sensitized TTA-UC systems.

1-5-2. Perovskite nanocrystals

Perovskite is a class of optoelectronic materials that have been intensively studied for various applications.[70-72] Three-dimensional metal halide perovskites have attracted significant attention as solar cell materials because of their tunable bandgaps and low exciton binding energy.[73-75] In nanometer-sized structures such as thin layers and nanocrystals, the spatial confinement of electrons and holes facilitates radiative recombination.[76, 77] Magneto-optical studies of perovskites showed that singlet and triplet excitons are generated after relaxation of the spin-antiparallel and spin-parallel electron-hole pairs, respectively.[78, 79] In addition, Becker *et al.* recently showed that the lowest-lying exciton in $CsPbX_3$ perovskite nanocrystals (PNCs) involves an optically bright triplet state, while that of most organic and inorganic semiconductor materials is known to be dark. Because of the small energy splitting of the singlet and triplet state in PNCs, these states undergo rapid population exchanges at room temperature.[80] These findings imply that PNCs are potentially capable of sensitizing molecular excited triplets, as is the case with metal chalcogenide QDs. A PNC-sensitized TTA-UC system is expected to have similar advantages to a QD-sensitized system.

Lead halide PNCs are photoluminescent with narrow full width at half maximum (FWHM) in the entire visible spectral range.[81, 82] Electronic surface passivation with wide-gap shell materials is not necessary for lead halide PNCs to achieve high photoluminescence quantum yield. This defect tolerance is attributed to their unique electronic structure in which defect states form only shallow traps or are enclosed in the conduction or valence band.[82] They possess two other advantages over metal chalcogenide QDs. The synthesis of PNCs is possible even under ambient conditions, while synthesizing QDs involves high-temperature reactions under an inert atmosphere. Bandgap tuning is easily accomplished by varying the halide composition in the precursors for the synthesis or by conducting post-synthesis anion exchange, although exacting size control is required in the case of QDs.[82]

Earlier studies demonstrated the extraction of triplet energy from 2-dimensional (2D) perovskites. The excited triplet state of naphthalene chromophores in organic-inorganic hybrid perovskite was generated by TET from inorganic layers.[83, 84] Younts *et al.* recently reported the formation of excited triplet states in a $(MA)_2Pb(SCN)_2I_2$ 2D perovskite film ($MA = CH_3NH_3^+$) and subsequent interfacial TET to an adjacent organic layer of rubrene or 9,10-bis(phenylethenyl)-anthracene as well as to perylene solution. TTA-UC emission from perylene was observed after selective excitation of 2D perovskite film using a 570 nm laser.[85]

Our group demonstrated the first example of triplet sensitization by PNCs for TTA-UC (Figure 1-8).[86] We used cesium lead halide $CsPb(Br/I)_3$ PNCs as inorganic triplet sensitizers. The surface was modified with energy transmitter ligands, 2-(4-(10-phenylanthracen-9-yl)-phenyl)ethan-1-amine (AEDPA). Under excitation at 532 nm, UC emission was observed from a deaerated solution of AEDPA-modified $CsPb(Br/I)_3$ and DPA in toluene, which showed UC efficiency of 1.3%. The transmitter molecule was found to play a crucial role in the TET process as observed in QD-sensitized TTA-UC because as-synthesized PNCs are also capped with long-chain passivating ligands. Importantly, this system showed red (635 nm)-to-blue (434 nm) TTA-UC with a large anti-Stokes shift of 0.90 eV, thanks to the small energy loss in the triplet sensitization process.

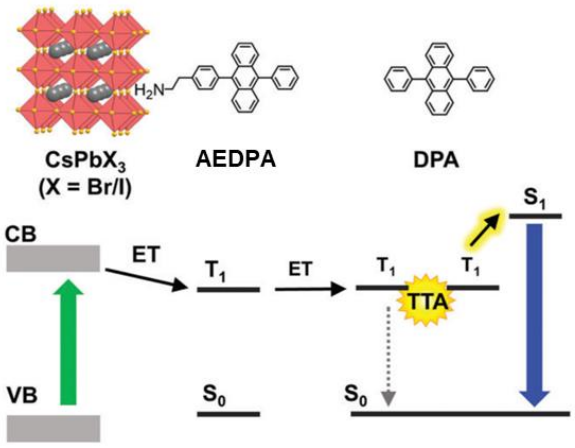

Figure 1-8. Scheme for TTA-UC sensitized by $CsPbX_3$ perovskite nanocrystals.[86]

The work described in Chapter 3 is the first demonstration of visible-to-UV TTA-UC sensitized by PNCs.[87] We generalized our previous work[86] by using lead halide PNCs with a different halide composition. The strategy of triplet energy relay by surface-attached transmitter molecules was also verified to work. We observed blue (488 nm)-to-UV (363 nm) TTA-UC with a large anti-Stokes shift of 0.88 eV. The details are discussed in Chapter 3.

Triplet energy transfer from PNCs to surface-bound acceptors has been confirmed by recent transient absorption spectroscopy studies by Wu and co-workers.[88, 89] They prepared $CsPbBr_3$ PNCs of varying sizes and modified the surface with 1-pyrenecarboxylic acid and 1-naphthalenecarboxylic acid. They directly monitored the dynamics of interfacial TET, and found quantum confinement to be essential for efficient TET. The TET rates scaled approximately linearly with the carrier probability density at the surface. This result was consistent with a Dexter-type TET mechanism that relies on the donor-acceptor wave function overlaps. After our report on the first example of visible-to-UV TTA-UC sensitized by PNCs, the authors also demonstrated efficient visible (443 nm)-to-UV (355 nm) TTA-UC.[90]

1-6. Overview of thesis

The aim of this work was to develop triplet sensitization processes in TTA-UC systems for the extension of anti-Stokes shift (Figure 1-9).

In Chapter 2, CdSe/ZnS core-shell quantum dots (QDs) were used as a triplet sensitizer for TTA-UC. This mechanism involves absorption of incident light by QDs followed by interfacial energy transfers from QDs to the triplet states of an emitter, and then TTA. There is no significant energy loss from ISC, which makes it possible to achieve a larger anti-Stokes shift compared with conventional TTA-UC systems sensitized by molecular sensitizers.

In Chapter 3, $CsPb(Cl/Br)_3$ perovskite nanocrystals (PNCs) were employed as another type of inorganic triplet sensitizer and the first example of visible-to-UV TTA-UC sensitized by PNCs was demonstrated. This system has a similar mechanism and similar advantage to the QD-sensitized system described in Chapter 2. The surface modification of PNCs with energy transmitter ligands played a key role in effective triplet sensitization, resulting in high UC efficiency.

Chapter 4 describes a new concept for sensitizer-free TTA-UC, in which excited triplet states of emitter molecules are generated by direct singlet-to-triplet (S-T) absorption. This system does not contain any energy-loss processes during ISC and TET, and is expected to offer a larger anti-Stokes shift than sensitized TTA-UC systems. Sensitizer-free TTA-UC was observed for crystals of brominated anthracene and perylene derivatives, which showed NIR-to-visible UC with remarkably large anti-Stokes shifts.

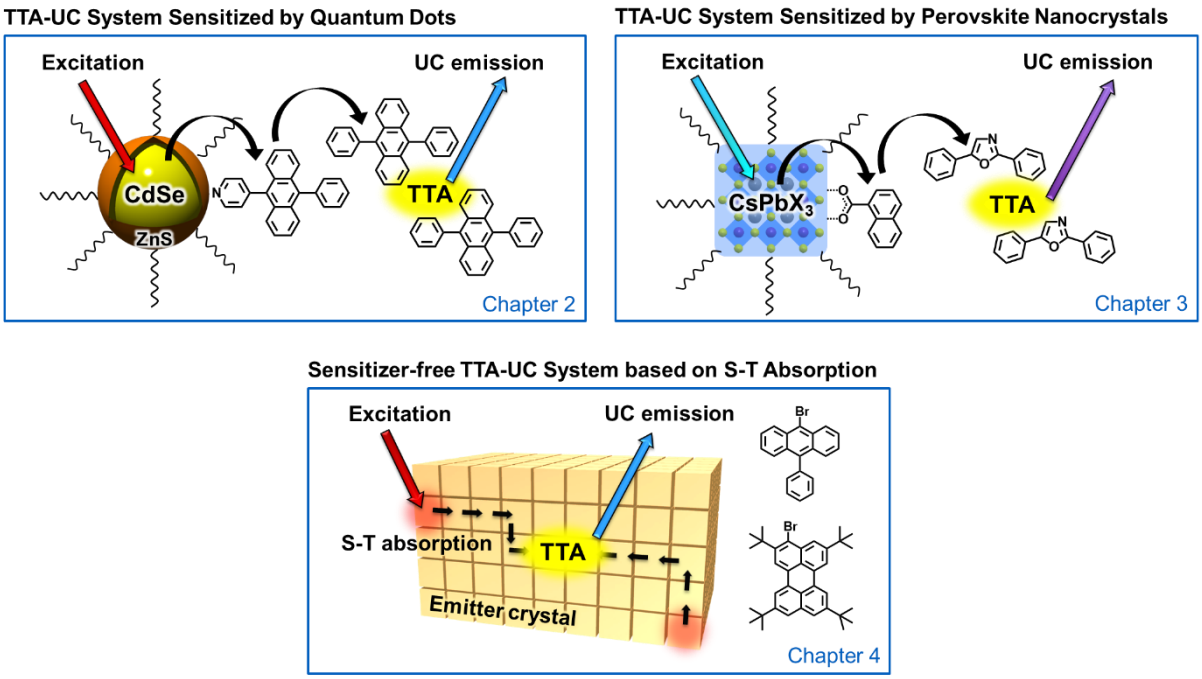

Figure 1-9. Schematic illustrations of the studies described.

References

[1] G. W. Crabtree, N. S. Lewis, *Phys. Today* **2007**, *60*, 37-42.

[2] T. F. Schulze, T. W. Schmidt, *Energy Environ. Sci.* **2015**, *8*, 103-125.

[3] W. Shockley, H. J. Queisser, *J. Appl. Phys.* **1961**, *32*, 510-519.

[4] T. Trupke, M. A. Green, P. Würfel, *J. Appl. Phys.* **2002**, *92*, 4117-4122.

[5] S. Baluschev, T. Miteva, V. Yakutkin, G. Nelles, A. Yasuda, G. Wegner, *Phys. Rev. Lett.* **2006**, *97*, 143903.

[6] T. N. Singh-Rachford, F. N. Castellano, *Coord. Chem. Rev.* **2010**, *254*, 2560-2573.

[7] J. Z. Zhao, S. M. Ji, H. M. Guo, *RSC Adv.* **2011**, *1*, 937-950.

[8] A. Monguzzi, R. Tubino, S. Hoseinkhani, M. Campione, F. Meinardi, *Phys. Chem. Chem. Phys.* **2012**, *14*, 4322-4332.

[9] Y. C. Simon, C. Weder, *J. Mater. Chem.* **2012**, *22*, 20817-20830.

[10] J. H. Kim, J. H. Kim, *J. Am. Chem. Soc.* **2012**, *134*, 17478-17481.

[11] Q. Liu, B. R. Yin, T. S. Yang, Y. C. Yang, Z. Shen, P. Yao, F. Y. Li, *J. Am. Chem. Soc.* **2013**, *135*, 5029-5037.

[12] N. Yanai, N. Kimizuka, *Chem. Commun.* **2016**, *52*, 5354-5370.

[13] N. Kimizuka, N. Yanai, M. Morikawa, *Langmuir* **2016**, *32*, 12304-12322.

[14] K. Kamada, Y. Sakagami, T. Mizokuro, Y. Fujiwara, K. Kobayashi, K. Narushima, S. Hirata, M. Vacha, *Mater. Horiz.* **2017**, *4*, 83-87.

[15] S. P. Hill, K. Hanson, *J. Am. Chem. Soc.* **2017**, *139*, 10988-10991.

[16] V. Gray, K. Moth-Poulsen, B. Albinsson, M. Abrahamsson, *Coord. Chem. Rev.* **2018**, *362*, 54-71.

[17] N. Yanai, N. Kimizuka, *Acc. Chem. Res.* **2017**, *50*, 2487-2495.

[18] H. Dong, L. -D. Sun, C. -H. Yan, *Chem. Soc. Rev.* **2015**, *44*, 1608-1634.

[19] J. Zhou, Q. Liu, W. Feng, Y. Sun, F. Y. Li, *Chem. Rev.* **2015**, *115*, 395-465.

[20] C. Ye, L. Zhou, X. Wang, Z. Liang, *Phys. Chem. Chem. Phys.* **2016**, *18*, 10818-10835.

[21] T. C. Wu, D. N. Congreve, M. A. Baldo, *Appl. Phys. Lett.* **2015**, *107*, 031103.

[22] J. Peng, X. Guo, X. Jiang, D. Zhao, Y. Ma, *Chem. Sci.* **2016**, *7*, 1233-1237.

[23] N. Yanai, M. Kozue, S. Amemori, R. Kabe, C. Adachi, N. Kimizuka, *J. Mater. Chem. C* **2016**, *4*, 6447-6451.

[24] D. Wei, F. Ni, Z. Zhu, Y. Zou, C. Yang, *J. Mater. Chem. C* **2017**, *5*, 12674-12677.

[25] Q. Chen, Y. Liu, X. Guo, J. Peng, S. Garakyaraghi, C. M. Papa, F. N. Castellano, D. Zhao, Y. Ma, *J. Phys. Chem. A* **2018**, *122*, 6673-6682.

[26] W. Chen, F. Song, S. Tang, G. Hong, Y. Wu, X. Peng, *Chem. Commun.* **2019**, *55*, 4375-4378.

[27] H. Uoyama, K. Goushi, K. Shizu, H. Nomura, C. Adachi, *Nature* **2012**, *492*, 234-238.

[28] S. Amemori, Y. Sasaki, N. Yanai, N. Kimizuka, *J. Am. Chem. Soc.* **2016**, *138*, 8702-8705.

[29] Y. Sasaki, S. Amemori, H.I Kouno, N. Yanai, N. Kimizuka, *J. Mater. Chem. C* **2017**, *5*, 5063-5067.

[30] D. Liu, Y. Zhao, Z. Wang, K. Xu, J. Zhao, *Dalton Trans.* **2018**, *47*, 8619-8628.

[31] Y. Wei, M. Zheng, L. Chen, X. Zhou, S. Liu, *Dalton Trans.* **2019**, *48*, 11763-11771.

[32] Y. Sasaki, M. Oshikawa, P. Bharmoria, H. Kouno, A. Hayashi-Takagi, M. Sato, I. Ajioka, N. Yanai, N.

Kimizuka, *Angew. Chem. Int. Ed.* **2019**, *58*, 17827-17833.

[33] S. Lamansky, P. Djurovich, D. Murphy, F. Abdel-Razzaq, H. E. Lee, C. Adachi, P. E. Burrows, S. R. Forrest, M. E. Thompson, *J. Am. Chem. Soc.* **2001**, *123*, 4304-4312.

[34] S. Altobello, R. Argazzi, S. Caramori, C. Contado, S. Da Fre, P. Rubino, C. Chone, G. Larramona, C. A. Bignozzi, *J. Am. Chem. Soc.* **2005**, *127*, 15342-15343.

[35] T. Kinoshita, J. Fujisawa, J. Nakazaki, S. Uchida, T. Kubo, H. Segawa, *J. Phys. Chem. Lett.* **2012**, *3*, 394-398.

[36] T. Kinoshita, J. T. Dy, S. Uchida, T. Kubo, H. Segawa, *Nat. Photonics* **2013**, *7*, 535-539.

[37] X. Zhang, S. E. Canton, G. Smolentsev, C. J. Wallentin, Y. Liu, Q. Kong, K. Attenkofer, A. B. Stickrath, M. W. Mara, L. X. Chen, K. Warnmark, V. Sundstrom, *J. Am. Chem. Soc.* **2014**, *136*, 8804-8809.

[38] P. Duan, N. Yanai, N. Kimizuka, *J. Am. Chem. Soc.* **2013**, *135*, 19056-19059.

[39] H. Kouno, T. Ogawa, S. Amemori, P. Mahato, N. Yanai, N. Kimizuka, *Chem. Sci.* **2016**, *7*, 5224-5229.

[40] S. Baluschev, V. Yakutkin, G. Wegner, B. Minch, T. Miteva, G. Nelles, A. Yasuda, *J. Appl. Phys.* **2007**, *101*, 023101.

[41] O. V. Mikhnenko, P. W. M. Blom, T.-Q. Nguyen, *Energy Environ. Sci.* **2015**, *8*, 1867-1888.

[42] R. Vadrucci, C. Weder, Y. C. Simon, *J. Mater. Chem. C* **2014**, *2*, 2837-2841.

[43] G. F. Moore, I. H. Munro, *Nature* **1965**, *208*, 772-773.

[44] V. Ern, H. Bouchriha, M. Bisceglia, S. Arnold, M. Schott, *Phys. Rev. B* **1973**, *8*, 6038-6042.

[45] L. Peter, G. Vaubel, *Chem. Phys. Lett.* **1973**, *21*, 158-160.

[46] N. J. Turro, V. Ramamurthy, J. C. Scaiano, *Modern Molecular Photochemistry of Organic Molecules*, University Science Books, Sausalito, CA, **2010**.

[47] J. Han, Y. Jiang, A. Obolda, P. Duan, F. Li, M. Liu, *J. Phys. Chem. Lett.* **2017**, *8*, 5865-5870.

[48] Z. Wang, J. Zhao, M. Di Donato, G. Mazzone, *Chem. Commun.* **2019**, *55*, 1510-1513.

[49] C. Fan, L. Wei, T. Niu, M. Rao, G. Cheng, J. J. Chruma, W. Wu, C. Yang, *J. Am. Chem. Soc.* **2019**, *141*, 15070-15077.

[50] G. D. Scholes, *Adv. Funct. Mater.* **2008**, *18*, 1157-1172.

[51] J. Kim, C. Y. Wong, G. D. Ssholes, *Acc. Chem. Res.* **2009**, *42*, 1037-1046.

[52] M. Tabachnyk, B. Ehrler, S. Gelinas, M. L. Bohm, B. J. Walker, K. P. Musselman, N. C. Greenham, R. H. Friend, A. Rao, *Nat. Mater.* **2014**, *13*, 1033-1038.

[53] N. J. Thompson, M. W. Wilson, D. N. Congreve, P. R. Brown, J. M. Scherer, T. S. Bischof, M. Wu, N. Geva, M. Welborn, T. V. Voorhis, V. Bulovic, M. G. Bawendi, M. A. Baldo, *Nat. Mater.* **2014**, *13*, 1039-1043.

[54] Z. Huang, X. Li, M. Mahboub, K. M. Hanson, V. M. Nichols, H. Le, M. L. Tang, C. J. Bardeen, *Nano Lett.* **2015**, *15*, 5552-5557.

[55] M. Wu, D. N. Congreve, M. W. B. Wilson, J. Jean, N. Geva, M. Welborn, T. Van Voorhis, V. Bulović, M. G. Bawendi, M. A. Baldo, *Nat. Photonics* **2016**, *10*, 31-34.

[56] C. Mongin, S. Garakyaraghi, N. Razgoniaeva, M. Zamkov, F. N. Castellano, *Science* **2016**, *351*, 369-372.

[57] K. Okumura, K. Mase, N. Yanai, N. Kimizuka, *Chem. Eur. J.* **2016**, *22*, 7721-7726.

[58] X. G. Peng, M. C. Schlamp, A. V. Kadavanich, A. P. Alivisatos, *J. Am. Chem. Soc.* **1997**, *119*, 7019-7029.

[59] J. J. Li, Y. A. Wang, W. Z. Guo, J. C. Keay, T. D. Mishima, M. B. Johnson, X. G. Peng, *J. Am. Chem. Soc.* **2003**, *125*, 12567-12575.

[60] M. A. Boles, D. Ling, T. Hyeon, D. V. Talapin, *Nat. Mater.* **2016**, *15*, 364.

[61] Z. A. Peng, X. G. Peng, *J. Am. Chem. Soc.* **2001**, *123*, 1389-1395.

[62] L. Nienhaus, M. Wu, V. Bulovic, M. A. Baldo, M. G. Bawendi, *Dalton Trans.* **2018**, *47*, 8509-8516.

[63] M. Mahboub, Z. Huang, M. L. Tang, *Nano. Lett.* **2016**, *16*, 7169-7175.

[64] V. Gray, P. Xia, Z. Huang, E. Moses, A. Fast, D. A. Fishman, V. I. Vullev, M. Abrahamsson, K. Moth-Poulsen, M. Lee Tang, *Chem. Sci.* **2017**, *8*, 5488-5496.

[65] Z. Huang, P. Xia, N. Megerdich, D. A. Fishman, V. I. Vullev, M. L. Tang, *ACS Photonics* **2018**, *5*, 3089-3096.

[66] Z. Huang, D. E. Simpson, M. Mahboub, X. Li, M. L. Tang, *Chem. Sci.* **2016**, *7*, 4101-4104.

[67] X. Li, Z. Huang, R. Zavala, M. L. Tang, *J. Phys. Chem. Lett.* **2016**, *7*, 1955-1959.

[68] X. Li, A. Fast, Z. Huang, D. A. Fishman, M. L. Tang, *Angew. Chem. Int. Ed.* **2017**, *56*, 5598-5602.

[69] Z. Huang, M. L. Tang, *J. Am. Chem. Soc.* **2017**, *139*, 9412-9418.

[70] J. S. Manser, J. A. Christians, P. V. Kamat, *Chem. Rev.* **2016**, *116*, 12956-13008.

[71] Y. Zhao, K. Zhu, *Chem. Soc. Rev.* **2016**, *45*, 655-689.

[72] S. A. Veldhuis, P. P. Boix, N. Yantara, M. Li, T. C. Sum, N. Mathews, S. G. Mhaisalkar, *Adv. Mater.* **2016**, *28*, 6804-6834.

[73] H.-S. Kim, S. H. Im, N.-G. Park, *J. Phys. Chem. C* **2014**, *118*, 5615-5625.

[74] S. D. Stranks, H. J. Snaith, *Nat. Nanotechnol.* **2015**, *10*, 391-402.

[75] B. Saparov, D. B. Mitzi, *Chem. Rev.* **2016**, *116*, 4558-4596.

[76] G. Li, Z. K. Tan, D. Di, M. L. Lai, L. Jiang, J. H. Lim, R. H. Friend, N. C. Greenham, *Nano Lett.* **2015**, *15*, 2640-2644.

[77] Z. Xiao, R. A. Kerner, L. Zhao, N. L. Tran, K. M. Lee, T.-W. Koh, G. D. Scholes, B. P. Rand, *Nat. Photonics* **2017**, *11*, 108-115.

[78] C. Zhang, D. Sun, C. X. Sheng, Y. X. Zhai, K. Mielczarek, A. Zakhidov, Z. V. Vardeny, *Nat. Phys.* **2015**, *11*, 427-434.

[79] Y. C. Hsiao, T. Wu, M. Li, B. Hu, *Adv. Mater.* **2015**, *27*, 2899-2906.

[80] M. A. Becker, R. Vaxenburg, G. Nedelcu, P. C. Sercel, A. Shabaev, M. J. Mehl, J. G. Michopoulos, S. G. Lambrakos, N. Bernstein, J. L. Lyons, T. Stoferle, R. F. Mahrt, M. V. Kovalenko, D. J. Norris, G. Raino, A. L. Efros, *Nature* **2018**, *553*, 189-193.

[81] M. V. Kovalenko, L. Protesescu, M. I. Bodnarchuk, *Science* **2017**, *358*, 745-750.

[82] Q. A. Akkerman, G. Raino, M. V. Kovalenko, L. Manna, *Nat. Mater.* **2018**, *17*, 394-405.

[83] M. Era, K. Maeda, T. Tsutsui, *Chem. Phys. Lett.* **1998**, *296*, 417-420.

[84] K. Ema, M. Inomata, Y. Kato, H. Kunugita, M. Era, *Phys. Rev. Lett.* **2008**, *100*, 257401.

[85] R. Younts, H.-S. Duan, B. Gautam, B. Saparov, J. Liu, C. Mongin, F. N. Castellano, D. B. Mitzi, K. Gundogdu, *Adv. Mater.* **2017**, *29*, 1604278.

[86] K. Mase, K. Okumura, N. Yanai, N. Kimizuka, *Chem. Commun.* **2017**, *53*, 8261-8264.

[87] K. Okumura, N. Yanai, N. Kimizuka, *Chem. Lett.* **2019**, *48*, 1347-1350.

[88] X. Luo, R. Lai, Y. Li, Y. Han, G. Liang, X. Liu, T. Ding, J. Wang, K. Wu, *J. Am. Chem. Soc.* **2019**, *141*, 4186-4190.

[89] Y. Han, X. Luo, R. Lai, Y. Li, G. Liang, K. Wu, *J. Phys. Chem. Lett.* **2019**, *10*, 1457-1463.

[90] S. He, X. Luo, X. Liu, Y. Li, K. Wu, *J. Phys. Chem. Lett.* **2019**, *10*, 5036-5040.

Chapter 2. Development of TTA-UC System Sensitized by Quantum Dots

2-1. Introduction

In this work, the surface of CdSe/ZnS core-shell QDs (denoted as csQD) was modified with energy transmitter molecules, 4-(10-phenylanthracene-9-yl)pyridine (PPA). PPA has a pyridyl moiety, and the nitrogen atom coordinates to the QD surface, which has been previously used in the post-modification of QDs.[1, 2]

Figure 2-1 shows the schematic illustration of the present system. In a mixed solution containing PPA-modified csQD and excess 9,10-diphenylanthracene (DPA), excitation of csQD is followed by energy transfer to the excited triplets of the surface-bound PPA, which relay the triplet energy to the free DPA molecules in the bulk. The subsequent TTA process leads to the UC emission. Interestingly, csQD-based system had a UC efficiency 50 times higher than the system using core-only CdSe QDs. Moreover, UC emission was also observed for the cast film of PPA-modified csQD and DPA.

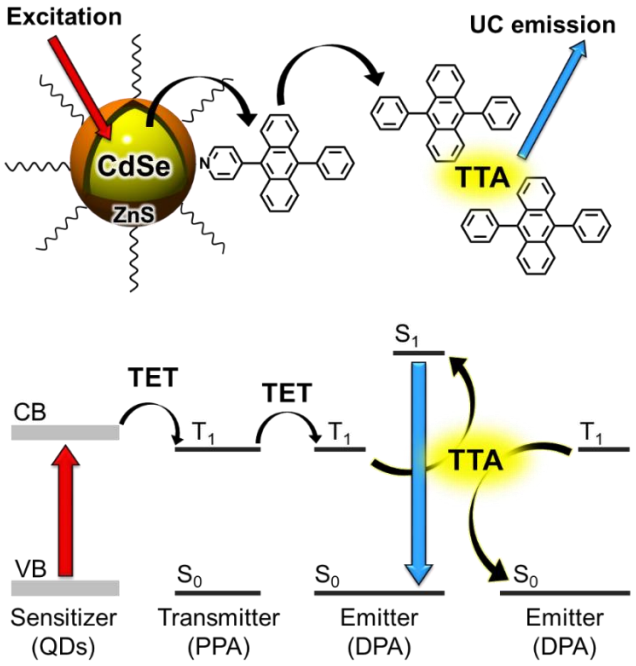

Figure 2-1. Scheme for TTA-UC sensitized by core-shell quantum dots.

2-2. Results and discussion

2-2-1. Surface modification of quantum dots with transmitter ligands

The transmitter ligand PPA in chloroform showed almost identical absorption and fluorescence spectra to those of DPA (Figure 2-2a). This indicates that the singlet energy level of PPA is basically same to that of DPA, which would also be the case for triplet energy levels.[3] The triplet energy level of transmitters should be carefully selected in consideration of the trade-off between triplet energy transfer (TET) efficiency and conservation of energy.[4] Although the energy cascade from QDs to emitter would be beneficial to realize high TET efficiency, such an energy-level alignment results in a smaller anti-Stokes shift because of the energy losses. In the current system, the transmitter and emitter molecules have an almost identical triplet level, which allows for a large anti-Stokes shift. This strategy shares similarity with the recent report by Nishimura *et al.*, in which NIR-to-visible TTA-UC with a large anti-Stokes shift of 0.86 eV was demonstrated.[5] A deaerated PPA solution in chloroform had a high fluorescence quantum yield of 86% ([PPA] = 10 mM).

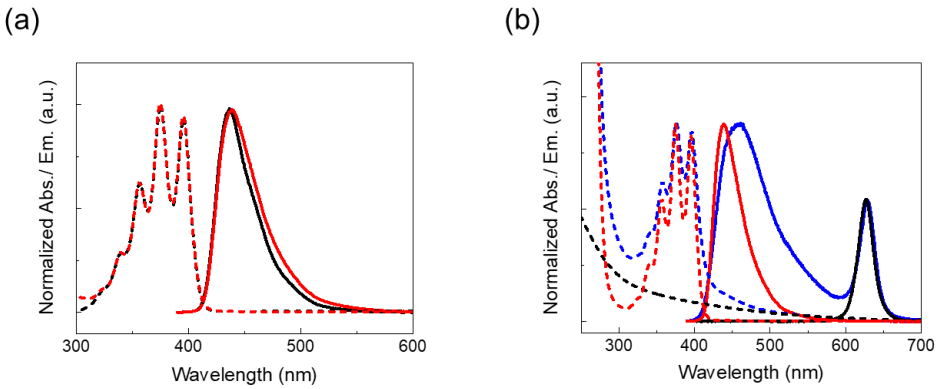

Figure 2-2. (a) Normalized absorption spectra (dashed lines) of DPA (black) and PPA (red) in chloroform (1 mM), and fluorescence spectra (solid lines, λ_{ex} = 370 nm) of DPA (black) and PPA (red) in chloroform (10 mM). (b) Normalized absorption (dashed lines) and emission (solid lines, λ_{ex} = 370 nm) spectra of csQD (black), PPA (red), PPA-csQD (blue) in chloroform.

The surface of csQD is initially capped by octadecylamine (ODA) according to the manufacturer. The surface modification with PPA was conducted (see Experimental section for details). The surface modification was confirmed by absorption, emission and ^{1}H NMR spectra. The absorption peaks of PPA were observed from the modified csQD solution, and they showed small red-shifts from 356, 375, and 395 nm to 357, 376, and 396 nm, which is attributable to the coordination to csQD (Figure 2-2b). The fluorescence band of PPA in the modified csQD showed a slight broadening and a peak shift from 439 to 458 nm, reflecting the heterogeneous environment for chromophores on the surface. The molar ratio of PPA to the original ligand ODA on the csQD surface was determined as 1:3 from ^{1}H NMR spectrum (Figure 2-3).

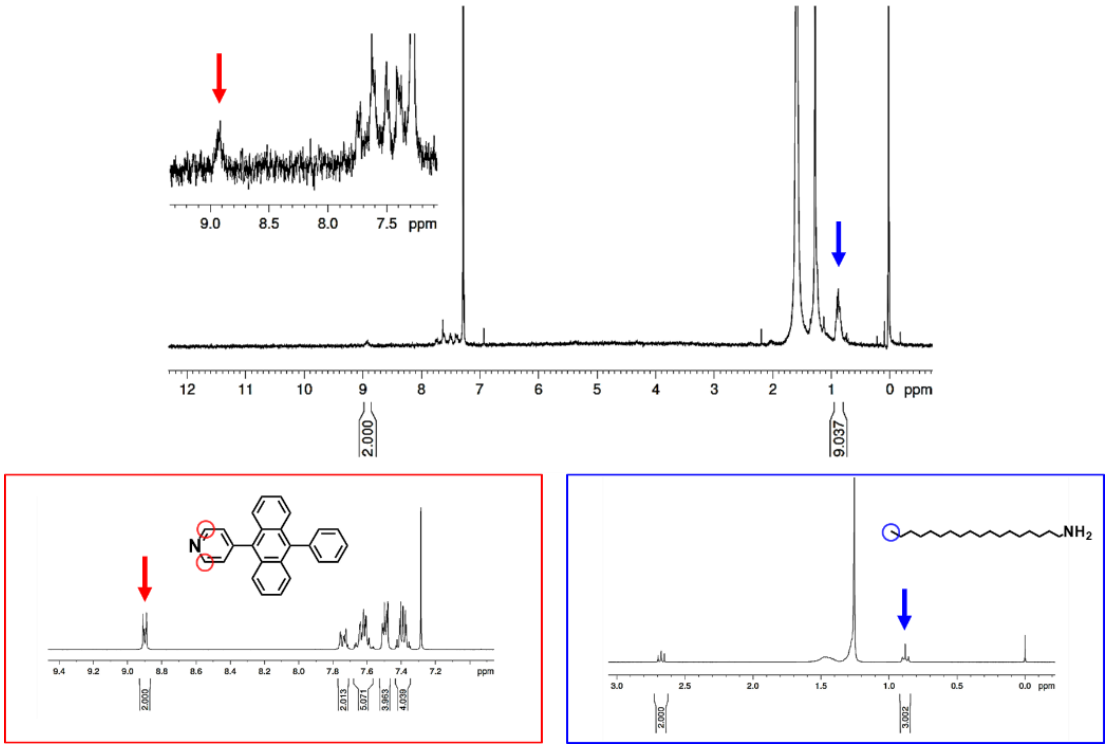

Figure 2-3. ^{1}H NMR spectrum (300 MHz, solvent: $CDCl_3$) of PPA-csQD. Inset: ^{1}H NMR spectra (300 MHz, solvent: $CDCl_3$) of PPA (red box) and ODA (blue box).

2-2-2. TTA-UC properties in solution system

First, UC measurement was conducted with a 532 nm continuous-wave laser as an excitation source. Under excitation at 532 nm, UC emission was clearly observed from a deaerated solution containing PPA-csQD and free DPA in chloroform (Figure 2-4). The UC emission peak at 433 nm indicates that the UC emission originates from free DPA molecules in the bulk solution.

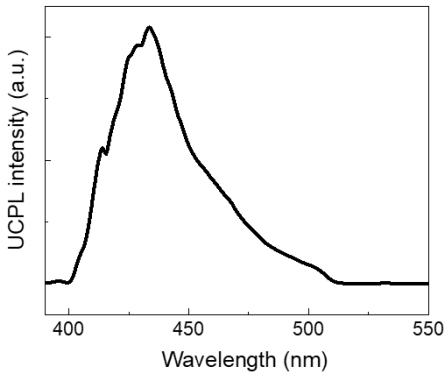

Figure 2-4. UC emission spectrum of PPA-csQD and DPA (10 mM) in deaerated chloroform using a laser with excitation wavelength λ_{ex} = 532 nm. A notch filter (λ = 532 nm) and a short-pass filter (λ = 510 nm) were used to remove the scattered incident light. The measurement was performed at room temperature under Ar atmosphere.

The UC emission had millisecond-scale decay profiles, indicating that the long-lived triplet-based mechanism (Figure 2-5a). The emitter triplet lifetime τ_T of 1.24 ms was obtained based on the relationship of $I_{UC}(t) \propto \exp(-2t/\tau_T)$.[6, 7]

The threshold excitation intensity I_{th} is a useful figure-of-merit of TTA-UC, at which the dependence of UC emission intensity on the excitation intensity changes from quadratic to linear.[8] The efficiency of TTA (Φ_{TTA}) depends on the triplet concentration in the system, and Φ_{TTA} becomes 50% at I_{th}. Figure 2-5b shows the double logarithmic plot of the UC emission intensity as a function of excitation intensity for the above UC sample. The slope showed a transition from 2 to 1, and the cross-section between these two lines gave the I_{th} value of 290 mW cm^{-2}. This I_{th} value is considerably smaller than those of the previous reports using core-only QDs (~10 W cm^{-2}).[9, 10]

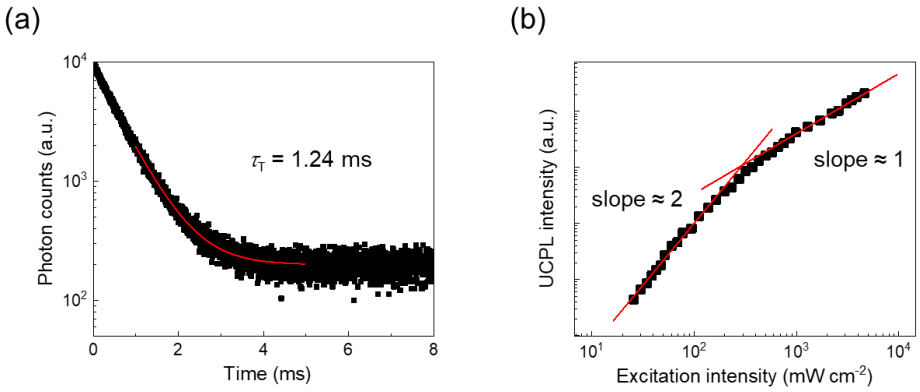

Figure 2-5. (a) Photoluminescence decay at 433 nm of PPA-csQD and DPA (10 mM) in deaerated chloroform under pulsed excitation at 531 nm. Single exponential fitting of the tail part (red line) provides the emitter triplet lifetime of 1.24 ms. The measurement was performed at room temperature under Ar atmosphere. (b) Dependence of UC photoluminescence intensity of PPA-csQD and DPA (10 mM) in deaerated chloroform at 433 nm on the excitation intensity. Red lines show the fitting results with slopes of 2 and 1. The measurement was performed at room temperature under Ar atmosphere.

For further confirmation of the mechanism illustrated in Figure 2-1, control experiments using solutions of the original ODA-capped csQD, PPA-csQD, or DPA were carried out. No UC emission was observed from the single-component solutions of the original csQD nor DPA. The PPA-csQD solution showed UC emission derived from PPA but its intensity was very weak. This is reasonable because PPA molecules are pinned to the csQD surface, which hinders TTA processes.

The UC mechanism is also supported by the photoluminescence decay measurements of csQD (Figure 2-6). The decay profile of the original ODA-capped csQD was not changed by the presence of excess DPA. In stark contrast, the decay became much faster in PPA-csQD, indicating the efficient energy transfer to the surface ligand PPA. Interestingly, coexistence of the excess DPA with PPA-csQD made the decay even faster. Therefore, the excited triplet energy should be transferred from surface-bound PPA to free DPA, followed by the inter-DPA annihilation process (Figure 2-1).

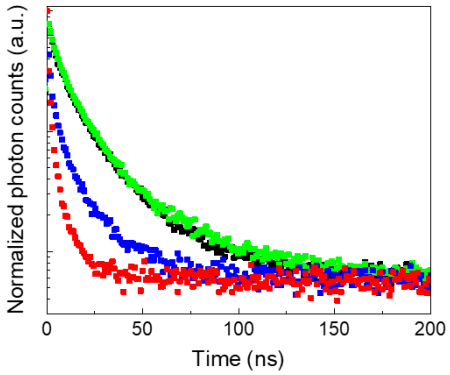

Figure 2-6. Photoluminescence decays at 630 nm of csQD (black), csQD and DPA (green), PPA-csQD (blue), and PPA-csQD and DPA (red) in deaerated chloroform under pulsed excitation at 590 nm. The measurements were performed at room temperature under Ar atmosphere.

To optimize the UC properties, we measured the TTA-UC quantum yield Φ_{UC} by changing the concentration of PPA-csQD. Φ_{UC} was determined relative to an external standard (see Experimental section for details). In general, the quantum yield is defined as the ratio of absorbed photons to emitted photons. The bimolecular TTA-UC process requires two photons to produce one higher-energy photon, and thus the theoretical maximum yield is 50%.[11, 12] In many reports, however, this value is multiplied by 2 to set the maximum efficiency as 100%. To avoid the confusion between these different definitions, the UC efficiency is written as Φ'_{UC} (= $2\Phi_{UC}$) when the maximum efficiency is normalized to be 100%. In all the measurement, a sufficiently high excitation intensity (2500 mW cm^{-2}) was used, at which the Φ'_{UC} of all the systems reached their saturated values. Starting from the identical stock solution of PPA-csQD, the relative concentration of PPA-csQD varied from 1 to 0.01, while fixing the concentration of DPA at 10 mM. As the relative concentration of PPA-csQD decreased from 1 to 0.05, the Φ'_{UC} value greatly increased from 0.012 to 1.4% (Figure 2-7a).

To understand this behavior, we examined the singlet and triplet lifetime of DPA. No significant change in the fluorescence lifetime of DPA was observed in the presence of PPA-csQD compared with that of the single-component solution of DPA (Figure 2-7b), indicating negligible back energy transfer from the excited singlet of DPA to PPA-csQD.

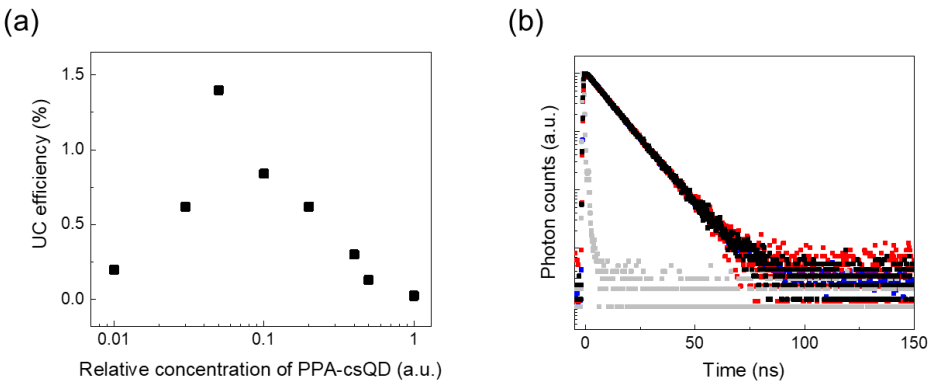

Figure 2-7. (a) Dependence of Φ'_{UC} on the relative concentration of PPA-csQD in deaerated chloroform. The measurements were performed at room temperature under Ar atmosphere. (b) Fluorescence decays at 433 nm of DPA (black), the mixture of PPA-csQD (the relative concentration of 0.5) and DPA (blue), and the mixture of PPA-csQD (the relative concentration of 0.05) and DPA (red) in deaerated chloroform under pulsed excitation at λ_{ex} = 365 nm. Gray dots represent the instrument response function (IRF). Three samples followed the single exponential behavior with lifetimes of 9.4 ns. The measurements were performed at room temperature under Ar atmosphere.

On the other hand, the triplet lifetime of DPA (τ_T) increased from 0.31 ms to 1.24 ms when the relative concentration of PPA-csQD was decreased from 0.5 to 0.05 (Figure 2-8). This result suggests the partial quenching of DPA triplet by PPA-csQD, which contributes to the reduced UC efficiency at high PPA-csQD concentration. Considering that the absorbance of the PPA-csQD (relative concentration of 1) at the peak of UC photoluminescence (433 nm) was 0.20, the re-absorption of upconverted emission by PPA-csQD might also take place. The further reduction of the relative PPA-csQD concentration from 0.05 to 0.01 decreased the Φ'_{UC}, probably due to the insufficient emitter triplet concentration for the efficient TTA process. Therefore, there is an optimal sensitizer concentration (the relative concentration of 0.05), which is used for all other UC measurements in this study.

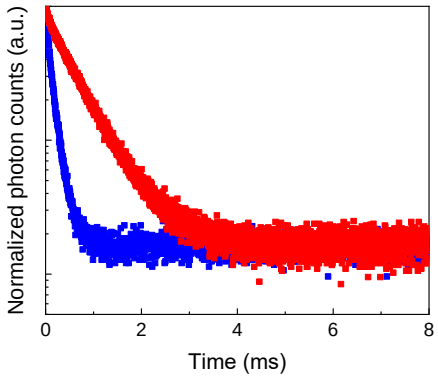

Figure 2-8. Photoluminescence decays at 433 nm of the mixture of PPA-csQD (the relative concentration of 0.5) and DPA (blue) and the mixture of PPA-csQD (the relative concentration of 0.05) and DPA (red) in deaerated chloroform under pulsed excitation at 531 nm, of which single exponential tail-fittings provide the triplet lifetimes of 0.31 ms and 1.24 ms, respectively. The measurements were performed at room temperature under Ar atmosphere.

To understand the effect of the surface modification with transmitter ligands for the TTA-UC properties described above, the control experiment was carried out by employing the original ODA-capped csQD as a sensitizer. The surface modification of csQD with transmitter ligands (PPA) reduced the I_{th} value from 810 to 290 mW cm^{-2}, and improved the UC efficiency (Φ'_{UC}) from 0.090 to 1.4% (Table 1). This should be mainly because of the enhanced TET efficiency by the conjugation of csQD with transmitter molecules.

Table 1. The effect of surface modification with transmitter ligands (PPA) and of QD structure (core-shell or core-only) upon I_{th} and Φ'_{UC} values.

QD structure	Emitter	I_{th} (mW cm^{-2})	Φ'_{UC} (%)
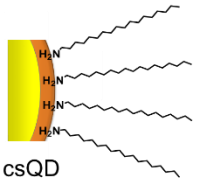 csQD	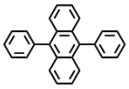	810	0.090
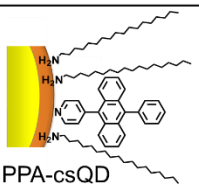 PPA-csQD	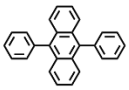	290	1.4
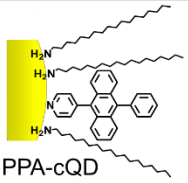 PPA-cQD	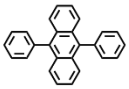	1290	0.026

Furthermore, the control experiment using core-only CdSe QDs (denoted as cQD) was also carried out to examine the effect of the shell structure. The validity of the cQD used here as a target for comparison with csQD was ascertained by ^{1}H NMR, emission and absorption spectra.

According to the manufacturer, the surface ligands of the cQD contain trioctylphosphine oxide (TOPO) as well as hexadecylamine (HDA). Although it was difficult to determine the molar ratio between TOPO and HDA on the surface due to the overlap of ^{1}H NMR spectra, the ratio between their alkyl chains and transmitter ligand PPA (3:1, Figure 2-9) was identical to the case of PPA-csQD (Figure 2-3). This result indicates the surface environment of PPA-modified cQD (PPA-cQD) is analogous to that of PPA-csQD.

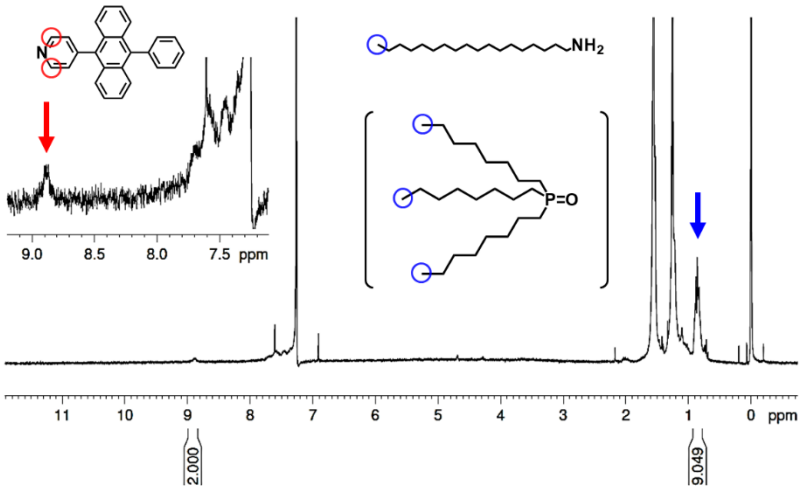

Figure 2-9. ^{1}H NMR spectrum (300 MHz, solvent: $CDCl_3$) of PPA-cQD.

The cQD showed an emission band at 643 nm (Figure 2-10), which is close to that of csQD (629 nm). In addition, PPA-cQD showed clear absorption peaks originated form PPA at 357, 367, and 396 nm (Figure 2-10), which are identical to those of PPA-csQD (Figure 2-2b). This result also supports the similar environment of PPA on csQD and cQD surfaces.

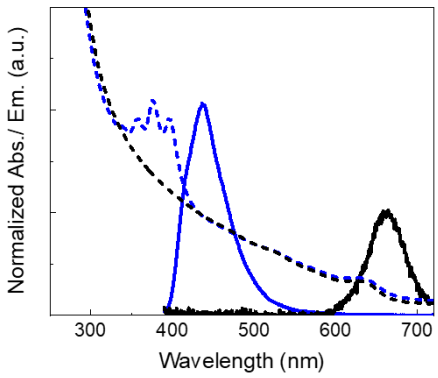

Figure 2-10. Normalized absorption (dashed lines) and emission (solid lines, λ_{ex} = 370 nm) spectra of cQD (black), PPA-cQD (blue) in chloroform.

The PPA-cQD/DPA system gave a much higher I_{th} value of 1290 mW cm^{-2} and a lower Φ'_{UC} of 0.026%, compared with the PPA-csQD/DPA system (Table 1). This is probably because core-only QDs have more surface defects than core-shell QDs, which decreases TET efficiency. This indicates that using core-shell QDs with fewer surface defects can improve the UC properties.

More importantly, TTA-UC was also achieved for the PPA-csQD/DPA system under excitation at 635 nm. UC emission was clearly observed at 433 nm (Figure 2-11), which is identical to the spectrum obtained under excitation at 532 nm. The anti-Stokes shift was calculated to be 0.91 eV. This result supports the advantage of TTA-UC system sensitized by QDs with a broadband absorption and without significant energy loss during intersystem crossing.

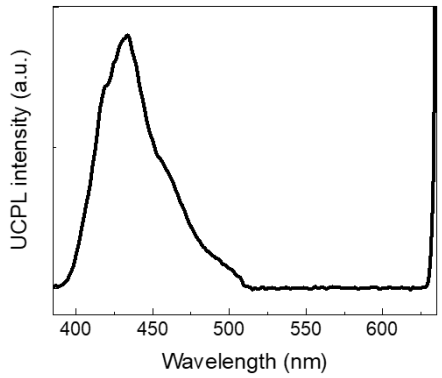

Figure 2-11. UC emission spectrum of PPA-csQD and DPA (10 mM) in deaerated chloroform using a laser with excitation wavelength λ_{ex} = 635 nm. Short-pass filters (λ = 510 nm, λ = 625 nm) were used to remove the scattered incident light. The measurement was performed at room temperature under Ar atmosphere.

2-2-3. TTA-UC properties in solid system

The UC emission at 433 nm was clearly observed for the cast film of PPA-csQD and DPA under excitation at both 532 nm and 635 nm, respectively (Figure 2-12). However, both UC emission and csQD emission became weaker with time under continuous laser irradiation. While further efforts to suppress the photo-degradation of csQD are required, our approach provide an important step towards the efficient TTA-UC in the solid state based on core-shell QD sensitizers.

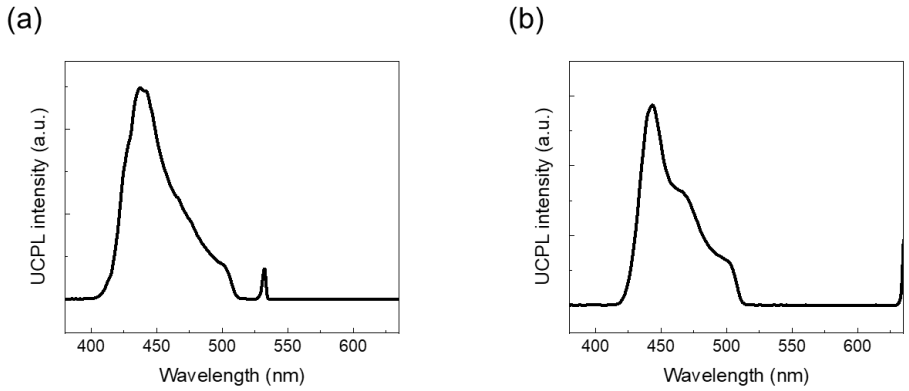

Figure 2-12. UC emission spectra of the solid samples. (a) λ_{ex} = 532 nm, excitation intensity = 8.6 W cm^{-2}. A notch filter (λ = 532 nm) and a short-pass filter (λ = 510 nm) were used to remove the scattered incident light. (b) λ_{ex} = 635 nm, excitation intensity = 62.0 W cm^{-2}. Short-pass filters (λ = 510 nm, λ = 610 nm, λ = 625 nm) were used to remove the scattered incident light. The measurements were performed at room temperature under Ar atmosphere.

2-3. Conclusion

In conclusion, TTA-UC system sensitized by core-shell QDs was firstly developed here. The surface modification of core-shell QDs with transmitter molecules and the presence of excess emitter molecules in solution facilitated the successive energy-transfer relay from QDs to the transmitter ligand, and then to the free emitters that were used for TTA process. There is an optimal concentration of core-shell QDs, at which the UC efficiency was enhanced and the I_{th} value was lowered. Furthermore, it was indicated that the fewer surface defects of core-shell QDs allow for the much lower I_{th} and higher Φ'_{UC} compared with the system using core-only QDs. Whereas further improvement of Φ'_{UC} and I_{th} values is required, the present work offers a promising strategy of using surface-functionalized core-shell QDs as triplet sensitizers for TTA-UC. Recent reports demonstrated that the QD sensitizers enable the upconversion of near-infrared (NIR) light into visible light,[10] which has been difficult to achieve with conventional molecular sensitizers. The combination of these advances and our findings may lead to the highly efficient NIR-to-visible TTA-UC at weak excitation intensity.

For future development of this work, the directional control of triplet diffusion would be an effective strategy. In the current system, back energy transfer from emitter (DPA) triplets to sensitizers (PPA-csQD) was one of the primary causes that constrain the energy transfer efficiency, which result in relatively low UC efficiency. This issue can be solved with the controlled triplet diffusion by introducing energy gradients to allow triplet species to escape from sensitizers within their long lifetime. For example, building a multi-layer structure in the solid system is a conceivable way to apply energy cascades, where the triplet diffusion layer exists between the sensitizer layer and the emitter (annihilator) layer.

2-4. Experimental

Materials

All reagents and solvents for synthesis and sample preparation were used as received without further purification. 9-Bromo-10-phenylanthracene (>98%), 4-pyridylboronic acid (contains varying amounts of anhydride) and 9,10-diphenylanthracene (DPA, >95%) were purchased from TCI.

Synthesis of 4-(10-phenylanthracene-9-yl)pyridine

4-(10-Phenylanthracene-9-yl)pyridine (PPA) was synthesized by modifying the reported methods of 9-(4-formylphenyl)-10-(4-pyridyl)anthracene[13] and 4-(anthracene-9-yl)pyridine.[14] Under Ar atmosphere, 9-bromo-10-phenylanthracene (666.4 mg, 2.00 mmol), 4-pyridylboronic acid (245.7 mg, 2.00 mmol), K_2CO_3 (1.386 g, 10 mmol), $Pd(PPh_3)_4$ (46.6 mg, 0.04 mmol), two drops of Aliquat 336 and degassed THF/H_2O (2:1, 15 mL) were added to a reaction tube. This mixture was heated (130 °C) by microwave (Biotage Initiator 2.5) for 5 h. The obtained slurry was extracted with ethyl acetate (150 mL), washed with brine, and dried over Na_2SO_4. After filtration, washed with ethylacetate and evaporated to dryness under reduced pressure, column chromatography (silica gel, dichloromethane) and recrystallization from hot acetone gave pale yellow powder (473.7 mg, 1.43 mmol, 71.5%).

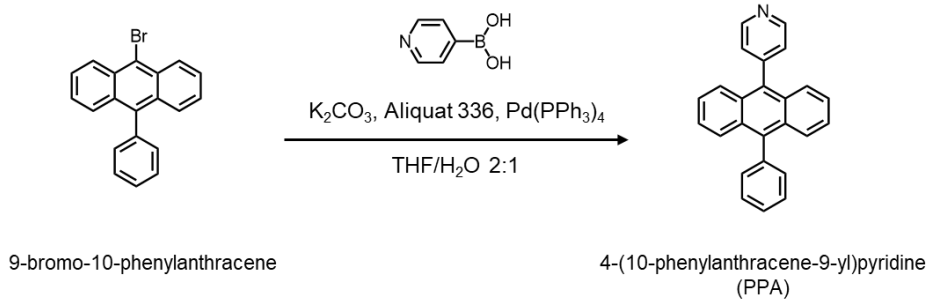

Figure 2-13. Scheme for the synthesis of PPA.

^{1}H NMR (300 MHz, $CDCl_3$, TMS standard)

δ = 8.88 (dd, J_1 = 4.35 Hz, J_2 = 1.59 Hz, 2H), 7.75-7.67 (m, 2H), 7.65-7.53 (m, 5H), 7.51-7.42 (m, 4H), 7.41-7.31 ppm (m, 4H).

Elemental analysis

Calculated (%) for $C_{25}H_{17}N$: C 90.60, H 5.17, N 4.23; Found: C 90.47, H 5.13, N 4.26.

Surface modification procedure

In an Ar-filled glovebox (oxygen concentration <0.1 ppm), CdSe/ZnS core-shell quantum dots (2.0 mg, stabilized with octadecylamine, fluorescence peak at λ_{em} = 630 nm, Sigma-Aldrich, denoted as csQD) and PPA (10.1 mg) were dissolved in chloroform (3.3 mL). The resulting solution was heated at 40 °C for 4 h under stirring, followed by stirring at room temperature for overnight. After being taken out from the glovebox, acetone (7.5 mL) was added. After centrifugation, orange-colored precipitate was obtained, and the supernatant was then removed. The precipitate, washed with acetone to remove free PPA, was dried under reduced pressure, giving PPA-modified csQD. In the glovebox, the resulting PPA-csQD was dissolved in chloroform (4.0 mL). The absorbance at 532 nm of this stock solution was 0.0069. This solution of PPA-csQD was stored at room temperature under light-shielded conditions. The same process was also conducted for CdSe core-only quantum dots (stabilized with hexadecylamine and trioctylphosphine oxide, fluorescence peak at λ_{em} = 640 nm, Sigma-Aldrich).

Sample preparation for TTA-UC measurements (solution)

The sample preparation was carried out in an Ar-filled glovebox. The PPA-csQD chloroform stock solution was diluted 20-fold with chloroform (otherwise the relative concentration is noted), and the DPA (10 mM) was added. The prepared solution samples were sealed in quartz cells of 1 mm thickness.

Sample preparation for TTA-UC measurements (solid)

The sample preparation was carried out in an Ar-filled glovebox. The PPA-csQD chloroform stock solution was diluted 10-fold with chloroform, and the DPA (100 mM) was added. The obtained solution (0.2 mL) was spin-coated (150 rpm) on a glass substrate, dried, and sealed under Ar atmosphere.

Measurement of UC efficiency

The Φ'_{UC} was determined relative to a standard (Rhodamine B) according to the following equation,

$$\Phi'_{UC} = 2\Phi_{std}\left(\frac{A_{std}}{A_{UC}}\right)\left(\frac{F_{UC}}{F_{std}}\right)\left(\frac{I_{std}}{I_{UC}}\right)\left(\frac{\eta_{UC}}{\eta_{std}}\right)^2$$

where Φ, A, F, I, and η represent quantum yield, absorbance at the excitation wavelength, integrated photoluminescence spectral profile, excitation intensity, and the refractive index of solvent, respectively.[15] The subscripts "UC" and "std" denote the parameters of the upconversion and standard systems, respectively.

Characterization

Elemental analysis was conducted at the Elemental Analysis Center, Kyushu University. ^{1}H NMR (300 MHz) spectra were measured on a Bruker DRX-spectrometer using TMS as the internal standard. UV-vis absorption spectra were recorded on a JASCO V-670 or JASCO V-770 spectrophotometer. Emission spectra were measured by using a PerkinElmer LS55 spectrophotometer with a 1 mm path length cell. The samples were excited at an incidence angle of 45º to the quartz cell surface, and the emission was detected along the normal. The absolute quantum yields were measured in an integrating sphere using a Hamamatsu Photonics absolute quantum yield measurement system. Time-resolved photoluminescence lifetime measurements were carried out by using a time-correlated single photon counting lifetime spectroscopy system, HAMAMATSU Quantaurus-Tau C11567-01 (for UC photoluminescence lifetime) / C11367-02 (for fluorescence lifetime).

For TTA-UC emission measurements, diode lasers (532 nm, 635 nm, RGB Photonis) were used as excitation sources. The laser power was controlled by combining a software (Ltune) and a variable neutral density filter, and measured using a PD300-UV photodiode sensor (OPHIR Photonics). The laser beam was focused on a sample using a lens. The diameter of the laser beam ($1/e^2$) was measured at the sample position using a CCD beam profiler SP620 (OPHIR Photonics). The emitted light was collimated by an achromatic lens, the excitation light was removed using short-pass filters, and the emitted light was again focused by an achromatic lens to an optical fiber connected to a multichannel detector MCPD-9800 (Otsuka Electronics).

References

[1] X. Luo, P. Liu, N. T. N. Truong, U. Farva, C. Park, *J. Phys. Chem. C* **2011**, *115*, 20817-20823.

[2] K. Susumu, E. Oh, J. B. Delehanty, F. Pinaud, K. B. Gemmill, S. Walper, J. Breger, M. J. Schroeder, M. H. Stewart, V. Jain, C. M. Whitaker, A. L. Huston, I. L. Medintz, *Chem. Mater.* **2014**, *26*, 5327-5344.

[3] V. Gray, D. Dzebo, A. Lundin, J. Alborzpour, M. Abrahamsson, B. Albinsson, K. Moth-Poulsen, *J. Mater. Chem. C* **2015**, *3*, 11111-11121.

[4] Z. Huang, M. L. Tang, *J. Am. Chem. Soc.* **2017**, *139*, 9412-9418.

[5] N. Nishimura, J. R. Allardice, J. Xiao, Q. Gu, V. Gray, A. Rao, *Chem Sci* **2019**, *10*, 4750-4760.

[6] M. Pope, C. E. Swenberg, *Electronic processes in organic crystals and polymers*, Oxford University Press, New York, **1999**.

[7] A. Monguzzi, F. Bianchi, A. Bianchi, M. Mauri, R. Simonutti, R. Ruffo, R. Tubino, F. Meinardi, *Adv. Energy Mater.* **2013**, *3*, 680-686.

[8] A. Monguzzi, J. Mezyk, F. Scotognella, R. Tubino, F. Meinardi, *Phys. Rev. B* **2008**, *78*, 195112.

[9] Z. Huang, X. Li, M. Mahboub, K. M. Hanson, V. M. Nichols, H. Le, M. L. Tang, C. J. Bardeen, *Nano Lett.* **2015**, *15*, 5552-5557.

[10] M. Wu, D. N. Congreve, M. W. B. Wilson, J. Jean, N. Geva, M. Welborn, T. Van Voorhis, V. Bulović, M. G. Bawendi, M. A. Baldo, *Nat. Photonics* **2016**, *10*, 31-34.

[11] A. Monguzzi, R. Tubino, S. Hoseinkhani, M. Campione, F. Meinardi, *Phys. Chem. Chem. Phys.* **2012**, *14*, 4322-4332.

[12] V. Gray, D. Dzebo, M. Abrahamsson, B. Albinsson, K. Moth-Poulsen, *Phys. Chem. Chem. Phys.* **2014**, *16*, 10345-10352.

[13] N. Mihara, Y. Teki, *Polyhedron* **2007**, *26*, 2142-2146.

[14] W. J. Ramsay, F. T. Szczypinski, H. Weissman, T. K. Ronson, M. M. Smulders, B. Rybtchinski, J. R. Nitschke, *Angew. Chem. Int. Ed.* **2015**, *54*, 5636-5640.

[15] T. N. Singh-Rachford, F. N. Castellano, *Coord. Chem. Rev.* **2010**, *254*, 2560-2573.

Chapter 3. Development of TTA-UC System Sensitized by Perovskite Nanocrystals

3-1. Introduction

Visible-to-UV TTA-UC has been relatively unexplored compared with the visible-to-visible and near infrared-to-visible TTA-UC mainly due to the absence of appropriate triplet sensitizers.[1-6] Gray *et al.* utilized CdS/ZnS core-shell nanocrystals as triplet sensitizer for visible (405 nm)-to-UV (355 nm) TTA-UC with a high UC efficiency of 5.2%.[6] It is however still desired to expand the variety of triplet sensitizer for more efficient visible-to-UV TTA-UC.

In this work, we demonstrated the first example of visible-to-UV TTA-UC sensitized by lead halide perovskite nanocrystals (PNCs). Excited triplets of 2,5-diphenyloxazole (PPO) are sensitized by $CsPb(Cl/Br)_3$ PNCs, and visible-to-UV TTA-UC with a high efficiency exceeding 4% is achieved. Efficient TTA-UC is obtained only in the presence of 1-naphthalenecarboxylic acid (NCA) attached to the PNCs surface, indicating that the NCA molecules serve as the energy transmitter between the sensitizer PNCs and emitter PPO (Figure 3-1).

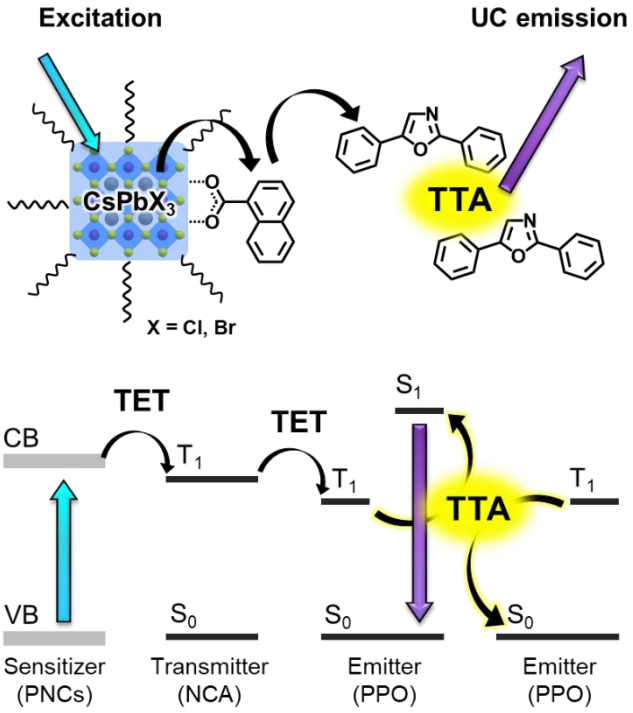

Figure 3-1. Scheme for visible-to-UV TTA-UC sensitized by lead halide perovskite nanocrystals.

3-2. Results and discussion

3-2-1. Surface modification of perovskite nanocrystals with transmitter ligands

$CsPb(Cl/Br)_3$ perovskite nanocrystals (PNCs) were synthesized according to the previous report with minor modifications (see Experimental section for details).[7] The obtained PNCs showed a photoluminescence peak at 480 nm (~2.6 eV, Figure 3-2a), which was tuned by controlling the mixing ratio of bromide and chloride precursors to have a sufficiently larger bandgap than the T_1 energy level of PPO (~2.3 eV).[8] The as-synthesized PNCs are initially covered with oleic acid and oleylamine. Our previous study elucidated that the energy transmitter molecules on the PNC surface play a key role in the triplet sensitization,[9] as is the case in TTA-UC sensitized by metal chalcogenide quantum dots (QDs).[10-13] While the excited state lifetime of these inorganic semiconductor nanocrystals is relatively short (~ns), the surface-bound transmitter allows the triplet energy transfer (TET) based on the electron-exchange Dexter mechanism. As a transmitter ligand, we used NCA with T_1 level of ~2.5 eV, which locates between the PNC bandgap (~2.6 eV) and PPO T_1 (~2.3 eV).[8] In the previous studies on QD-sensitized TTA-UC system, this energy cascade was proved to promote TET processes.[14] It has been reported that oleate molecules coordinate to the PNC surface during the synthesis of PNCs,[15, 16] and the surface-bound oleate ligands can be exchanged with other ligands having a carboxylate moiety.[17, 18] In this system, the transmitter ligands NCA would also coordinate to the PNC surface in the deprotonated form.

In the presence of NCA, no significant difference was observed in the absorption and emission spectral shapes of PNCs, suggesting that the PNC structure was well maintained (Figure 3-2a). This was also supported by transmission electron microscopy (TEM) measurements (Figures 3-2b and 3-2c). The morphology of PNCs was preserved after the surface modification with NCA, and the size was not changed between before (9.1 ± 0.8 nm) and after (9.4 ± 0.8 nm) the modification. On the other hand, photoluminescence of PNCs was partially quenched; the photoluminescence quantum yield of PNCs decreased from $\Phi_0 = 60\%$ to $\Phi = 41\%$. The maximum energy transfer efficiency (Φ_{ET}) was estimated as $\Phi_{ET} = 1-\Phi/\Phi_0 = 32\%$. Further optimization of PNC structure and surface chemistry would improve the energy transfer efficiency.

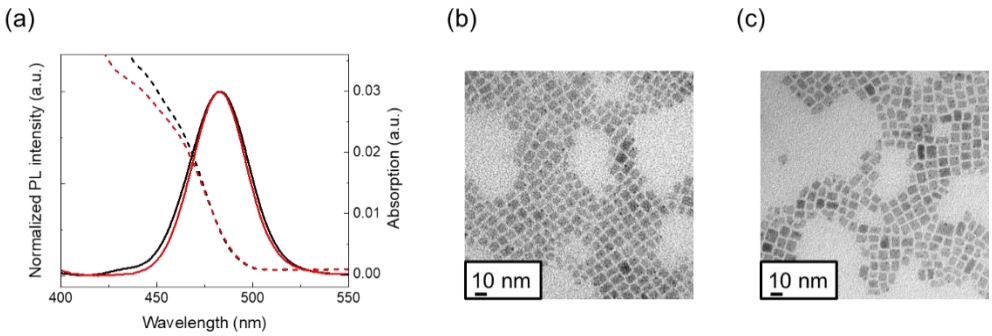

Figure 3-2. (a) Normalized absorption (dashed lines) and normalized photoluminescence (solid lines) spectra of as-synthesized PNCs (black) and NCA (5 mM)/PNCs (red). TEM images of (b) as-synthesized PNCs and (c) NCA (5 mM)/PNCs.

3-2-2. TTA-UC properties

Under excitation at 445 nm, a deaerated solution containing PNCs, NCA (5 mM) and PPO (50 mM) in toluene showed UC photoluminescence at 363 nm (Figure 3-3a). The peak position of UC emission matches well with the one of PPO fluorescence (Figure 3-3b). Meanwhile, two-component solutions of PNCs/NCA (5 mM) and PNCs/PPO (50 mM) showed no detectable UC photoluminescence (Figure 3-3a). These behaviors agree well with our previous work[9] and suggest that NCA and PPO function as the transmitter and emitter, respectively. The photo-excited energy is transferred from the PNCs to the excited triplet state of surface-bound NCA, which relays the triplet energy to PPO molecules and leads to TTA-UC emission from PPO (Figure 3-1).

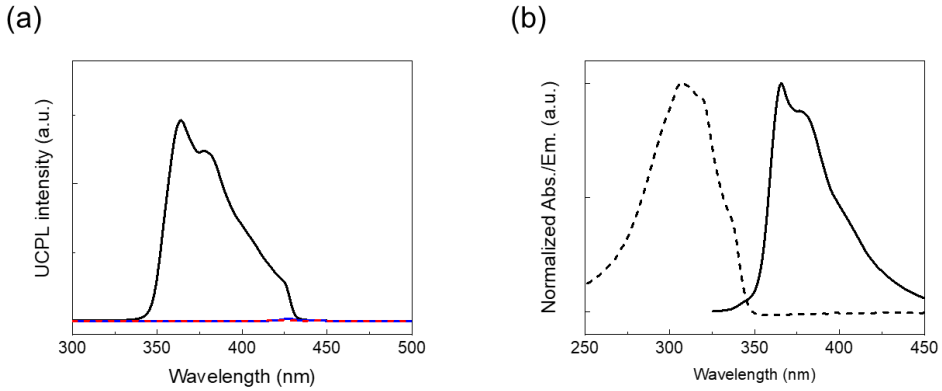

Figure 3-3. (a) UC photoluminescence spectra of PNCs/NCA/PPO (black), PNCs/NCA (blue) and PNCs/PPO (red, dashed line) in deaerated toluene using a 445 nm laser (102 W cm^{-2}). A short-pass filter (λ = 425 nm) was used to remove the scattered excitation light. The measurements were performed at room temperature under Ar atmosphere. (b) Absorption spectrum of PPO (100 μM) in chloroform (dashed line) and fluorescence spectrum of PPO (50 mM) in toluene (solid line).

The TTA-based UC mechanism was verified by the lifetime of UC emission and the excitation intensity dependence of UC emission intensity. The UC emission exhibited microsecond-scale decay profiles, indicating the mechanism via long-lived excited triplet states (Figure 3-4a). A triplet lifetime τ_T of 260 μs was obtained based on the relationship of $I_{UC}(t) \propto \exp(-2t/\tau_T)$.[19] UC photoluminescence spectra were measured at different excitation intensities. The dependence of the UC emission intensity on the excitation intensity changed from quadratic to linear, as generally observed for TTA-UC systems (Figure 3-4b).[20-22] The point of intersection between two fitting lines of slope 2 and 1 in the double-logarithmic plot gave a threshold excitation intensity I_{th} of 4.7 W cm^{-2}, which is comparable to the visible-to-UV TTA-UC sensitized by CdS/ZnS nanocrystals (2-3 W cm^{-2}).[6]

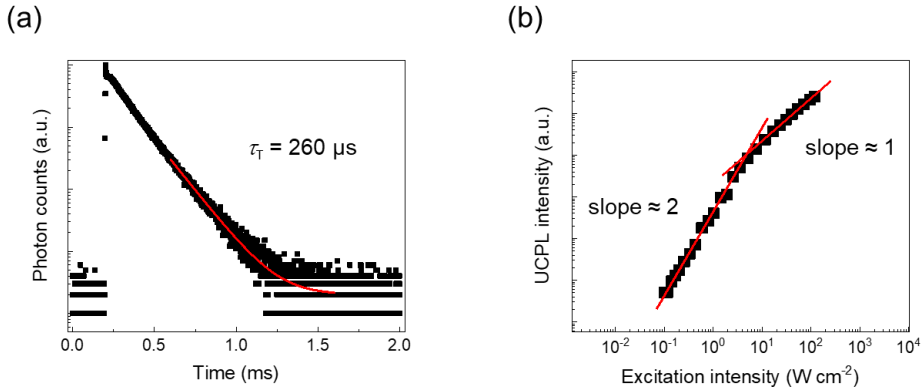

Figure 3-4. (a) Photoluminescence decay at 363 nm of PNCs/NCA/PPO in deaerated toluene under pulsed excitation at 445 nm. Single exponential fitting of the tail part (red line) provides the triplet lifetime of 260 μs. The measurement was performed at room temperature under Ar atmosphere. (b) Excitation intensity dependence of UC photoluminescence intensity of PNCs/NCA/PPO in deaerated toluene at 363 nm. Red lines show the fitting results with slopes of 2 and 1. The measurement was performed at room temperature under Ar atmosphere.

The excitation intensity dependence of UC efficiency (Φ'_{UC}) for the PNCs/NCA/PPO mixed solution was evaluated relative to a standard (Coumarin 6). The Φ'_{UC} value gradually increased with the increase of excitation intensity and exceeded 4% (Figure 3-5). The obtained Φ'_{UC} value is comparable to the record values of visible-to-UV TTA-UC sensitized by molecular sensitizers (3.9%)[4] and CdS/ZnS nanocrystals (5.2%),[6] proving the high triplet sensitization ability of PNCs.

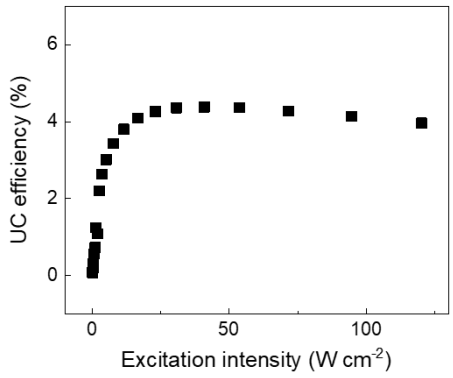

Figure 3-5. Excitation intensity dependence of UC efficiency (Φ'_{UC}) for PNCs/NCA/PPO in deaerated toluene. The measurement was performed at room temperature under Ar atmosphere.

To further confirm the UC mechanism illustrated in Figure 3-1, we carried out two control experiments. First, alternative transmitter ligands with different excited triplet levels, benzoic acid (BA) and 9-anthracenecarboxylic acid (ACA), were used to prove the importance of appropriate sensitizer/transmitter/emitter energy level alignment. The T_1 energy level of BA (~3.4 eV) is higher than the PNC bandgap (~2.6 eV), and the T_1 energy level of ACA (~1.8 eV) is lower than that of PPO (~2.3 eV).[8] No UC photoluminescence was observed for both of the PNCs/BA/PPO and PNCs/ACA/PPO solutions (Figure 3-6a). Second, to examine the effect of surface binding of transmitter molecules, naphthalene (NA) and 1-naphthaleneacetic acid (NAA) were used instead of NCA. From their similar absorption and fluorescence spectra (Figure 3-6b), NA and NAA are considered to have similar T_1 energy level (~2.6 eV).[8] While the PNCs/NAA/PPO solution showed visible-to-UV UC emission, no UC emission was observed from the PNCs/NA/PPO solution (Figure 3-6c), indicating that surface binding of transmitter molecules is essential for TET. The weaker UC emission intensity was observed for PNCs/NAA/PPO than PNCs/NCA/PPO, which would be attributed to the longer distance between PNCs and the naphthalene unit and/or the smaller driving energy for TET. Note that no appearance

changes of PNC solution such as turbidness was observed by the addition of BA, ACA, NA and NAA, which is similar to the PNC solution containing NCA. This suggests that the presence of these molecules does not damage the PNC structure.

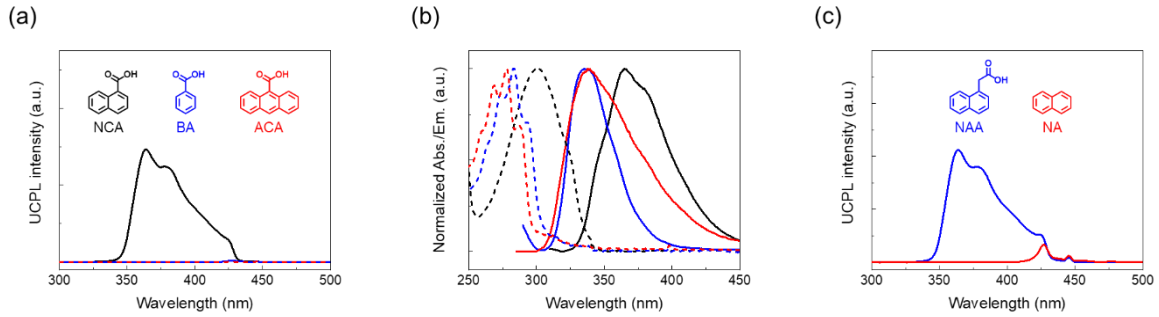

Figure 3-6. (a) UC photoluminescence spectra of PNCs/NCA/PPO (black), PNCs/BA/PPO (blue) and PNCs/ACA/PPO (red, dashed line) in deaerated toluene using a 445 nm laser (102 W cm^{-2}). A short-pass filter (λ = 425 nm) was used to remove the scattered excitation light. The measurements were performed at room temperature under Ar atmosphere. (b) Absorption (dashed line) and fluorescence (solid line) spectra of NCA (black), NAA (blue) and NA (red) in chloroform (100 μM). (c) UC photoluminescence spectra of PNCs/NAA/PPO (blue) and PNCs/NA/PPO (red) in deaerated toluene using a 445 nm laser (102 W cm^{-2}). A short-pass filter (λ = 425 nm) was used to remove the scattered excitation light. The measurements were performed at room temperature under Ar atmosphere.

Notably, even under excitation at 488 nm, PNCs/NCA/PPO system exhibited UC emission (Figure 3-7). The observed spectrum was identical to the spectrum obtained under excitation at 445 nm. In this case, the anti-Stokes shift was calculated to be 0.88 eV. This result confirms the benefit of PNC-sensitized TTA-UC system that have a broad absorption property and less energy loss resulting from intersystem crossing.

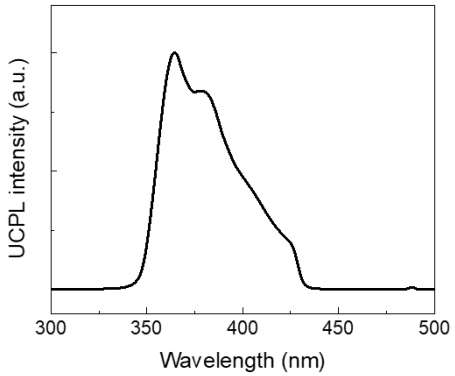

Figure 3-7. UC photoluminescence spectrum of PNCs/NCA/PPO in deaerated toluene using a 488 nm laser. A short-pass filter ($\lambda = 425$ nm) was used to remove the scattered excitation light. The measurement was performed at room temperature under Ar atmosphere.

3-3. Conclusion

In conclusion, we demonstrated the first example of visible-to-UV TTA-UC sensitized by lead halide perovskite nanocrystals (PNCs) and presented the generality of our previous study. The surface of $CsPb(Cl/Br)_3$ PNCs was modified with 1-naphthalenecarboxylic acid (NCA) as transmitter ligands. The T_1 level of NCA locates between the PNC bandgap and T_1 level of 2,5-diphenyloxazole (PPO), showing energy cascade to facilitate triplet energy transfer (TET). A series of control experiments clarified that the surface-bound NCA is crucial for the interfacial TET from sensitizer PNCs to emitter PPO. Under excitation at 445 nm, efficient TTA-UC with high Φ'_{UC} exceeding 4% was observed from a sensitizer (PNCs)/transmitter (NCA)/emitter (PPO) mixed solution. We also observed UC photoluminescence even under excitation at 488 nm, which gave a large anti-Stokes shift of 0.88 eV. This work proves the promising potential of perovskite nanocrystals as the next-generation triplet sensitizers.

In the current system, there is still room for improvement. Especially, the relatively low Φ_{ET} (~32%) is one of the issues to be solved. As exemplified in QD-sensitized TTA-UC system, the interface architecture of nanocrystal-transmitter hybrids is of significant importance for efficient TET. To further increase Φ_{ET} and consequent Φ'_{UC}, transmitter molecules should be newly designed considering several factors such as the triplet energy level, binding geometry, binding affinity and stability. Besides, exploration of other perovskite families would open a new avenue for constructing TTA-UC system with improved performances.

3-4. Experimental

Materials

All reagents and solvents were used as received otherwise noted. Cesium bromide (>99.0%), 2,5-diphenyloxazole (PPO, >99.0%), 1-naphthalenecarboxylic acid (NCA, >98.0%), benzoic acid (BA, >98.0%), 1-naphthaleneacetic acid (NAA, >98.0%), naphthalene (NA, >98.0%), 9-anthracenecarboxylic acid (ACA, >97.0%) and 3-(2-benzothiazolyl)-7-(diethylamino)coumarin (Coumarin 6, >98.0%) were purchased from TCI. Lead bromide (99.999%) was purchased from Alfa Aesar. Lead chloride (99.999%) and oleylamine (70%) were purchased from Sigma-Aldrich. Oleic acid was purchased from Kishida. Toluene (deoxygenated) and *N*,*N*-dimethylformamide (DMF, deoxygenated) were purchased from Wako.

Synthesis of $CsPb(Cl/Br)_3$ perovskite nanocrystals[7]

All the sample preparations were conducted in an Ar-filled glove box (oxygen concentration <0.1 ppm). As a precursor solution, CsBr (21.3 mg, 0.10 mmol), $PbBr_2$ (27.5 mg, 0.075 mmol) and $PbCl_2$ (7.0 mg, 0.025 mmol) were dissolved in 5 mL of DMF. 0.125 mL of oleylamine and 0.25 mL of oleic acid were added to the solution at 40 °C. 0.10 mL of this precursor solution was quickly added into 5 mL of toluene under vigorous stirring at room temperature. After 2 minutes, the obtained solution was filtered through a 0.2 μm PTFE syringe filter and diluted for two folds with a 10 mM oleylamine solution in toluene.

Sample preparation for TTA-UC measurements

2,5-Diphenyloxazole (PPO) and 1-naphthalenecarboxylic acid (NCA) were purified by recrystallization before use. Oleylamine and oleic acid were degassed by a vacuum pump, then introduced into the glove box. The prepared solution samples were sealed in quartz cells of 1 mm thickness in the glove box.

Characterization

Transmission electron microscope (TEM) images were taken by a JEOL JEM-2010. UV-vis absorption spectra were recorded on a JASCO V-670 or JASCO V-770 spectrophotometer. Emission spectra of perovskite nanocrystals were measured on a PerkinElmer LS55 spectrophotometer with a 1 mm path length cell. The samples were excited at an incidence angle of 45º to the quartz cell surface, and the emission was detected along the normal. Fluorescence spectrum of PPO was measured on a multichannel detector MCPD-9800 (Otsuka Electronics) with a 1 mm path length cell, using UV lamp

(λ = 254 nm) as an excitation source. The absolute quantum yields were measured in an integrating sphere using a Hamamatsu Photonics absolute quantum yield measurement system. Time-resolved photoluminescence measurements were carried out by using a time-correlated single photon counting lifetime spectroscopy system, Hamamatsu Quantaurus-Tau C11567-01 (for UC photoluminescence lifetime).

For TTA-UC emission measurements, diode lasers (445 nm, 488 nm, RGB Photonics) were used as excitation sources. The laser power was controlled by combining a software (Ltune) and a variable neutral density filter, and measured using a PD300-UV photodiode sensor (OPHIR Photonics). The laser beam was focused on a sample using a lens. The diameter of the laser beam ($1/e^2$) was measured at the sample position using a CCD beam profiler SP620 (OPHIR Photonics). The emitted light was collimated by an achromatic lens, the excitation light was removed using a short-pass filter (λ = 425 nm), and the emitted light was again focused by an achromatic lens to an optical fiber connected to a multichannel detector MCPD-9800 (Otsuka Electronics).

References

[1] W. Zhao, F. N. Castellano, *J. Phys. Chem. A* **2006**, *110*, 11440-11445.

[2] T. N. Singh-Rachford, F. N. Castellano, *J. Phys. Chem. A* **2009**, *113*, 5912-5917.

[3] P. Duan, N. Yanai, N. Kimizuka, *Chem. Commun.* **2014**, *50*, 13111-13113.

[4] N. Yanai, M. Kozue, S. Amemori, R. Kabe, C. Adachi, N. Kimizuka, *J. Mater. Chem. C* **2016**, *4*, 6447-6451.

[5] Q. Chen, Y. Liu, X. Guo, J. Peng, S. Garakyaraghi, C. M. Papa, F. N. Castellano, D. Zhao, Y. Ma, *J. Phys. Chem. A* **2018**, *122*, 6673-6682.

[6] V. Gray, P. Xia, Z. Huang, E. Moses, A. Fast, D. A. Fishman, V. I. Vullev, M. Abrahamsson, K. Moth-Poulsen, M. Lee Tang, *Chem. Sci.* **2017**, *8*, 5488-5496.

[7] X. Li, Y. Wu, S. Zhang, B. Cai, Y. Gu, J. Song, H. Zeng, *Adv. Funct. Mater.* **2016**, *26*, 2435-2445.

[8] M. Montalti, A. Credi, L. Prodi, M. T. Gandolfi, *Handbook of photochemistry, third edition*, CRC Press, Boca Raton, **2006**.

[9] K. Mase, K. Okumura, N. Yanai, N. Kimizuka, *Chem. Commun.* **2017**, *53*, 8261-8264.

[10] Z. Huang, X. Li, M. Mahboub, K. M. Hanson, V. M. Nichols, H. Le, M. L. Tang, C. J. Bardeen, *Nano Lett.* **2015**, *15*, 5552-5557.

[11] Z. Huang, X. Li, B. D. Yip, J. M. Rubalcava, C. J. Bardeen, M. L. Tang, *Chem. Mater.* **2015**, *27*, 7503-7507.

[12] C. Mongin, S. Garakyaraghi, N. Razgoniaeva, M. Zamkov, F. N. Castellano, *Science* **2016**, *351*, 369-372.

[13] K. Okumura, K. Mase, N. Yanai, N. Kimizuka, *Chem. Eur. J.* **2016**, *22*, 7721-7726.

[14] Z. Huang, M. L. Tang, *J. Am. Chem. Soc.* **2017**, *139*, 9412-9418.

[15] J. De Roo, M. Ibanez, P. Geiregat, G. Nedelcu, W. Walravens, J. Maes, J. C. Martins, I. Van Driessche, M. V. Kovalenko, Z. Hens, *ACS Nano* **2016**, *10*, 2071-2081.

[16] D. P. Nenon, K. Pressler, J. Kang, B. A. Koscher, J. H. Olshansky, W. T. Osowiecki, M. A. Koc, L. W. Wang, A. P. Alivisatos, *J. Am. Chem. Soc.* **2018**, *140*, 17760-17772.

[17] H. Lu, X. Chen, J. E. Anthony, J. C. Johnson, M. C. Beard, *J. Am. Chem. Soc.* **2019**, *141*, 4919-4927.

[18] X. Luo, R. Lai, Y. Li, Y. Han, G. Liang, X. Liu, T. Ding, J. Wang, K. Wu, *J. Am. Chem. Soc.* **2019**, *141*, 4186-4190.

[19] M. Pope, C. E. Swenberg, *Electronic processes in organic crystals and polymers*, Oxford University Press, New York, **1999**.

[20] A. Monguzzi, J. Mezyk, F. Scotognella, R. Tubino, F. Meinardi, *Phys. Rev. B* **2008**, *78*, 195112.

[21] Y. Y. Cheng, T. Khoury, R. G. C. R. Clady, M. J. Y. Tayebjee, N. J. Ekins-Daukes, M. J. Crossley, T. W. Schmidt, *Phys. Chem. Chem. Phys.* **2010**, *12*, 66-71.

[22] A. Haefele, J. Blumhoff, R. S. Khnayzer, F. N. Castellano, *J. Phys. Chem. Lett.* **2012**, *3*, 299-303.

Chapter 4. Development of Sensitizer-free TTA-UC System based on S-T Absorption

4-1. Introduction

In Chapter 2 and Chapter 3, TTA-UC systems based on inorganic sensitizers showed large anti-Stokes shifts by avoiding the energy loss in intersystem crossing process of sensitizers, which is generally inevitable in molecular sensitizers (Figure 4-1a). In this chapter, sensitizer-free TTA-UC system consisting only of brominated aromatic crystals is newly proposed for the further extension of anti-Stokes shifts in TTA-UC. This study focused on direct population of excited triplets through singlet-to-triplet (S-T) absorption in organic crystals. S-T absorption-based TTA-UC mechanism can circumvent the energy losses of ISC and TET, which potentially offers an extremely large anti-Stokes shift beyond the reach of common sensitized TTA-UC (Figure 4-1b).

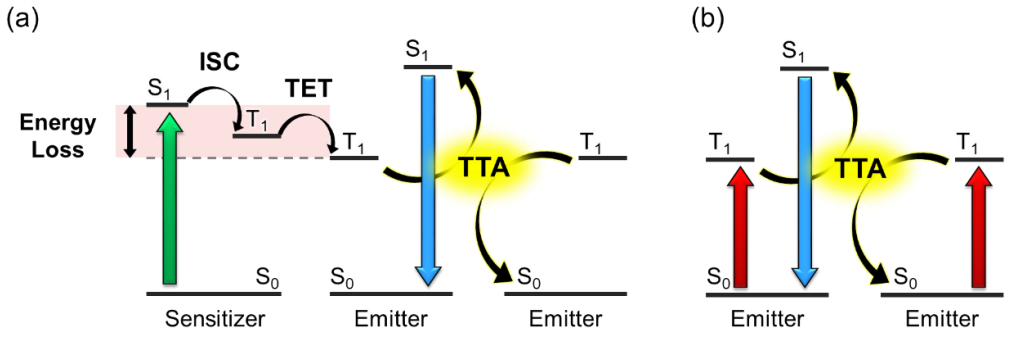

Figure 4-1. Schematic representations of (a) conventional sensitized TTA-UC and (b) sensitizer-free TTA-UC based on S-T absorption.

Since anthracene derivatives are the benchmark emitters in conventional sensitized TTA-UC, the concept of sensitizer-free S-T absorption-based UC was demonstrated by using three brominate anthracene derivatives, 9-bromoanthracene (BA), 9,10-dibromoanthracene (DBA) and 9-bromo-10-phenylanthracene (BPA). A near-infrared (NIR) light excitation (λ_{ex} = 724 nm) at relatively low intensity (~W cm^{-2}) populated triplet excitons in these crystals via direct excitation of S-T band, which was followed by triplet energy migration[1-7] and eventually TTA to show blue UC emission with a remarkably large anti-Stokes shift (Figure 4-2). Furthermore, the application of this approach to a brominated perylene derivative allowed for TTA-UC of longer wavelength NIR light (λ_{ex} = 856 nm) to green light with a large anti-Stokes shift, demonstrating the generality of the current approach.

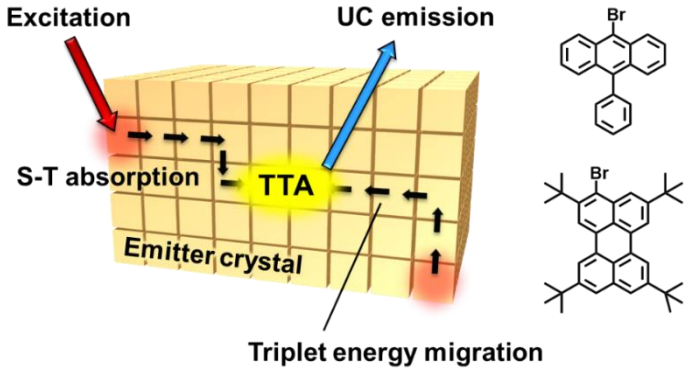

Figure 4-2. Scheme for S-T absorption-based UC in single-component organic crystals. Yellow boxes represent emitter molecules. The excited triplets are produced via S-T absorption, followed by triplet energy migration, TTA, and UC emission.

4-2. Results and discussion

4-2-1. Sensitizer-free TTA-UC properties of anthracene derivatives

The reported crystal structures of BA and DBA show the π-π staking of anthracene rings (Figures 4-3a and 4-3b).[8] The crystal structure of BPA was solved in this study (Figure 4-3c).[9] The twisted phenyl ring against anthracene moiety provides a slipped stacking of anthracene chromophores.

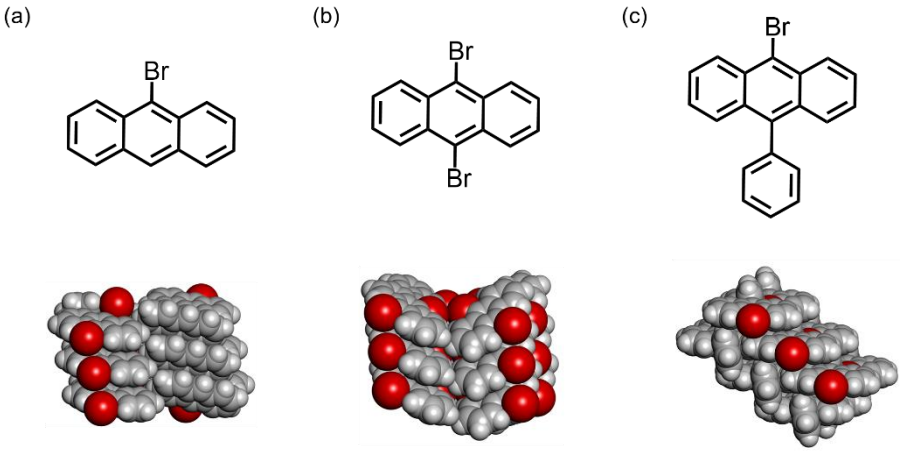

Figure 4-3. Chemical and crystal structures of (a) BA, (b) DBA and (c) BPA. Red, gray and white balls represent bromine, carbon and hydrogen atoms, respectively.

The phase purity of the crystals was confirmed by the good agreement between the experimental X-ray powder diffraction (XRPD) patterns and the simulation patterns obtained from the crystal structures (Figure 4-4).

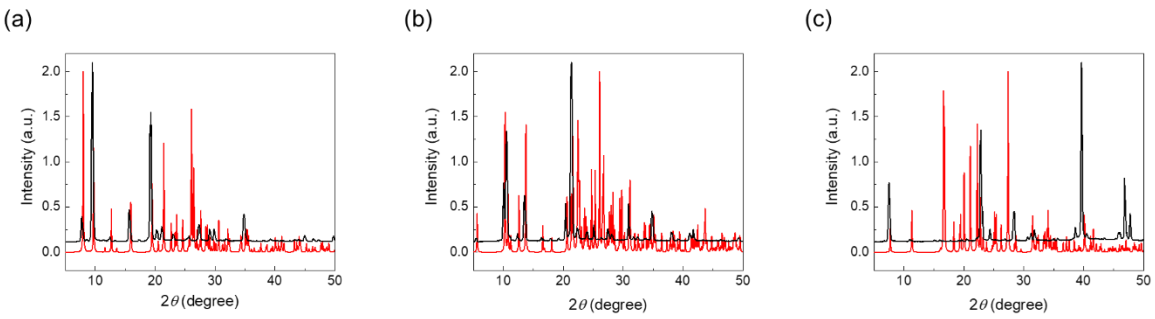

Figure 4-4. XRPD patterns (black lines) of (a) BA, (b) DBA and (c) BPA together with the simulated patterns (red lines) obtained from their crystal structures.

A series of basic photophysical characterizations were carried out for the three compounds both in solution and solid states. A chloroform solution of BA showed structured π-π* absorption bands at 353, 372 and 392 nm and emission peaks at 398, 421 and 446 nm (Figure 4-5a), which are typical for the molecularly dispersed anthracene chromophores. On the other hand, the emission spectrum in the solid state was red-shifted and became structureless, reflecting the presences of intermolecular interactions and self-absorption in the molecular crystals. Similar behaviors were also observed for DBA and BPA (Figures 4-5b and 4-5c).

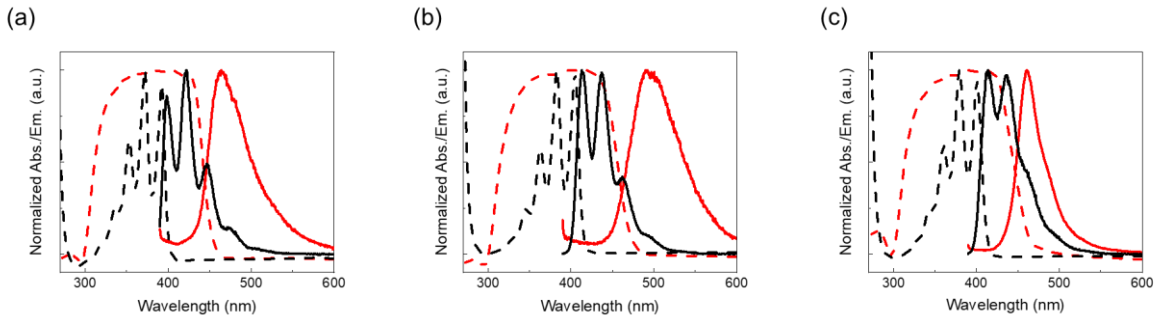

Figure 4-5. Normalized absorption (dashed lines) and fluorescence (solid lines) spectra of (a) BA, (b) DBA and (c) BPA in chloroform (black, 10 μM) and in the solid state (red).

For the upconversion measurements of anthracene derivatives, a 724 nm (~1.7 eV) continuous-wave laser was employed as an excitation source because it is known that the T_1 energy level of anthracene derivatives lies around at 1.7 eV.[10] The details of optical setup are described in the Experimental section. First, to build a base for S-T absorption-based UC under relatively low excitation intensity, UC measurements were carried out using crystals of non-brominated anthracene and BA under Ar atmosphere. Only a quite weak UC emission was observed from the crystalline anthracene under excitation at 724 nm (Figure 4-6, black). This is reasonable because spin-forbidden S-T absorption is usually very weak in the absence of heavy atoms. The use of higher-power light source leads to the direct population of triplets in anthracene crystals,[11] but such strong excitation is not desirable in many applications.

Interestingly, on the other hand, upconverted emission was clearly observed for BA crystals (Figure 4-6, red). The position of UC emission spectrum matches well with the fluorescence spectrum of crystalline BA (Figure 4-5a). The UC emission peaks of BA locates at 472 nm, exhibiting a large anti-Stokes shift of 0.92 eV. This result is significant because anthracene chromophores are usually not excited with such a long-wavelength NIR light. Although Pd(II) 1,4,8,11,15,18,22,25-octabutoxy phthalocyanine ($PdPc(OBu)_8$) is a widely-used sensitizer that can be excited by a 725 nm laser,[12] the succeeding ISC causes a fall of the T_1 energy level to 1.24 eV, which is much lower than the T_1 energy level of anthracene derivatives (~1.7 eV). This comparison highlights the advantage of sensitizer-free UC system that circumvents the energy losses unavoidable for the ISC and TET processes.

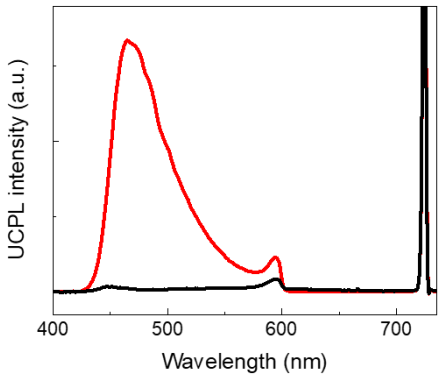

Figure 4-6. Photoluminescence spectra of BA crystals (red) and anthracene crystals (black) under Ar atmosphere upon excitation with a 724 nm laser at 145 W cm^{-2}. Scattered incident light and the residual phosphorescence were removed by short-pass filters (λ = 590 nm, λ = 690 nm). The measurements were performed at room temperature.

The mechanism of UC emission via TTA was confirmed by the excitation intensity dependence of the photoluminescence intensity and photoluminescence lifetime measurements. Figure 4-7 shows double logarithmic plots for the UC emission intensity as a function of excitation intensity, in which measurements were conducted up to the maximum output intensity of the employed laser (389 W cm^{-2}, Experimental section). The slope of 2 was observed for BA crystals, which is consistent with the quadratic dependence of biexciton TTA process.

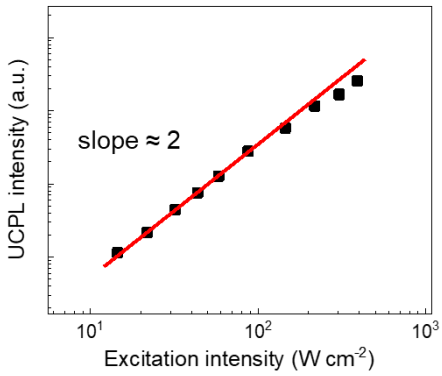

Figure 4-7. UC photoluminescence intensity for crystalline BA as a function of the excitation intensity (λ_{ex} = 724 nm). A red line shows the fitting result with slope of 2. The measurement was performed at room temperature under Ar atmosphere.

In addition, a pulsed excitation at 720 nm of the crystalline BA showed a decay profile of UC photoluminescence in the microsecond time scale (Figure 4-8, blue). It has been well documented that the excited triplet lifetime τ_T can be estimated by fitting the UC emission decay tail based on the relationship of $I_{UC}(t) \propto \exp(-2t/\tau_T)$.[13] At the decay tails, the triplet concentration is low enough to ignore the effect of TTA upon its decay kinetics. The fitting result gave τ_T of 123 μs, and the observed μs-scale lifetime supports that UC emission is produced through the long-lived excited triplet states. The occurrence of TTA based on the collision of two excited triplets was further confirmed by a phosphorescence lifetime measurement under the pulsed excitation at 720 nm. The BA crystals showed phosphorescence peaks at 705 nm and 790 nm (Figure 4-9). The single exponential fitting of phosphorescence decay at 790 nm ($I_{Phos}(t) \propto \exp(-t/\tau_T)$) gave τ_T of 119 μs for the crystals of BA (Figure 4-8, red). Similar to the case of UC emission decay, the tail part of phosphorescence decay is governed by thermal deactivation process and not affected by TTA. This is supported by the fact that the tail parts of UC and phosphorescence decays can be nicely fitted with single-exponential fittings. It is to note that the triplet lifetime determined from phosphorescence decay agrees well with that obtained from UC emission decay. This result demonstrates that both of phosphorescence and UC emission originate from the identical triplet species formed by direct S-T transition.

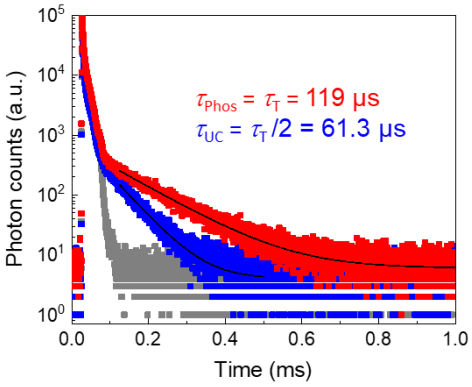

Figure 4-8. Photoluminescence decays at 470 nm (blue) and 790 nm (red) of crystalline BA under pulsed excitation at 720 nm. The black fitting curves were obtained by considering the relationship of $I_{UC}(t) \propto \exp(-2t/\tau_T)$ and $I_{Phos}(t) \propto \exp(-t/\tau_T)$. Gray dots represent the instrument response function (IRF). The measurements were performed at room temperature under Ar atmosphere.

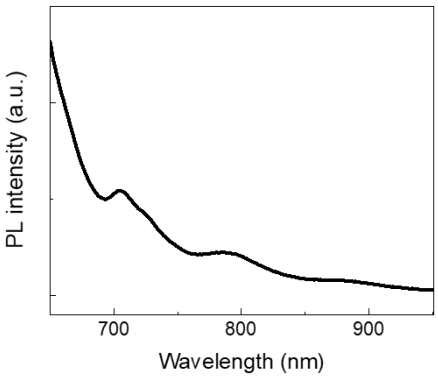

Figure 4-9. Photoluminescence spectrum of crystalline BA upon excitation with a 445 nm laser (I_{ex} = 1.53 W cm^{-2}). Peaks at 705 nm and 790 nm, observed as shoulder peaks of fluorescence and/or scattering light, are assignable as T_1-to-S_0 phosphorescence.[14] The measurement was performed at room temperature under Ar atmosphere.

Analogous upconversion behaviors were observed for DBA and BPA crystals, which showed large anti-Stokes shifts of 0.76 and 0.96 eV, respectively (Figures 4-10 and 4-11).

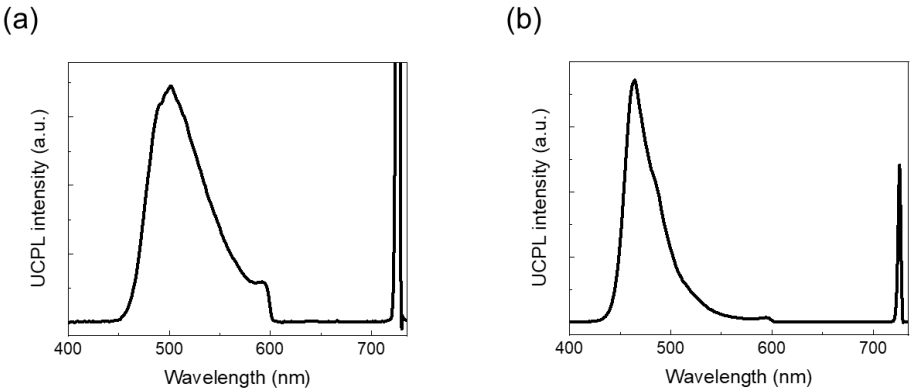

Figure 4-10. Photoluminescence spectra of (a) DBA and (b) BPA crystals upon excitation with a 724 nm laser. Scattered incident light and the residual phosphorescence were removed by short-pass filters (λ = 590 nm, λ = 690 nm). The measurements were performed at room temperature under Ar atmosphere.

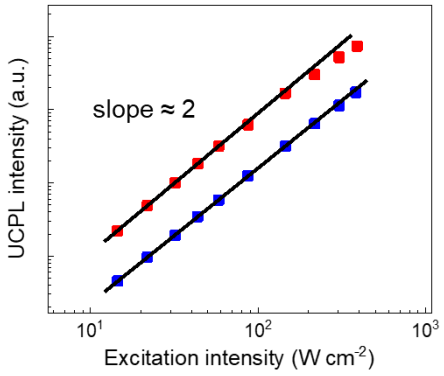

Figure 4-11. UC photoluminescence intensity for crystalline DBA (blue) and BPA (red) as a function of the excitation intensity (λ_{ex} = 724 nm). Black lines show the fitting result with slope of 2. The measurements were performed at room temperature under Ar atmosphere.

To further confirm the UC mechanism illustrated in Figure 4-2, and to exclude the possibility of two-photon absorption (TPA), we carried out excitation intensity dependence using other excitation wavelengths. The BA, DBA and BPA crystals showed UC photoluminescence under excitation with 635 nm and 532 nm lasers, indicating that the S-T absorption covers this wavelength region. Only the quadratic dependence of UC emission intensity on excitation intensity was observed under excitation at 724 nm, which is probably due to the power limitation of the laser source (Figure 4-7). In fact, the stronger excitation of BPA crystals at 532 nm enabled us to observe the slope change from quadratic to linear (Figure 4-12). This is a characteristic behavior for the TTA-mediated UC emission,[15] which cannot be explained by the TPA mechanism.

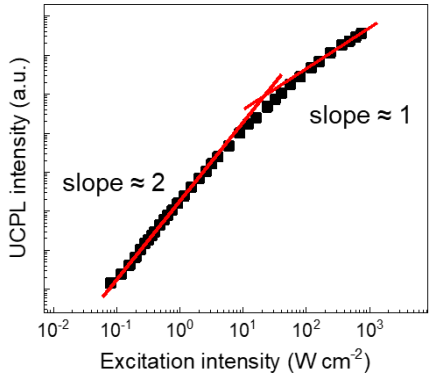

Figure 4-12. UC emission intensity for crystalline BPA as a function of the excitation intensity (λ_{ex} = 532 nm). Red lines show the fitting results with slopes of 2 and 1. The measurement was performed at room temperature under Ar atmosphere.

We also observed the effect of oxygen upon the UC emission. While weak in intensity, UC photoluminescence with a remarkably large anti-Stokes shift of 1.11 eV was observed for BPA in deaerated chloroform (100 mM) under excitation at 724 nm (Figure 4-13a, red). Similar to the solid-state system, the UC emission of the solution sample showed the quadratic dependence upon excitation intensity (Figure 4-13b). Importantly, the UC emission was totally quenched under aerated condition (Figure 4-13a, black). This result is consistent with the UC mechanism via the excited triplet states which are sensitive to molecular oxygen.[16] Interestingly, in contrast to the solution system, UC emission was observed from the solid-state system even under the aerated conditions. This result is in accord with earlier studies of air-stable phosphorescence from organic crystals, indicating that the oxygen diffusion is effectively prohibited in dense molecular arrangements.[17-21]

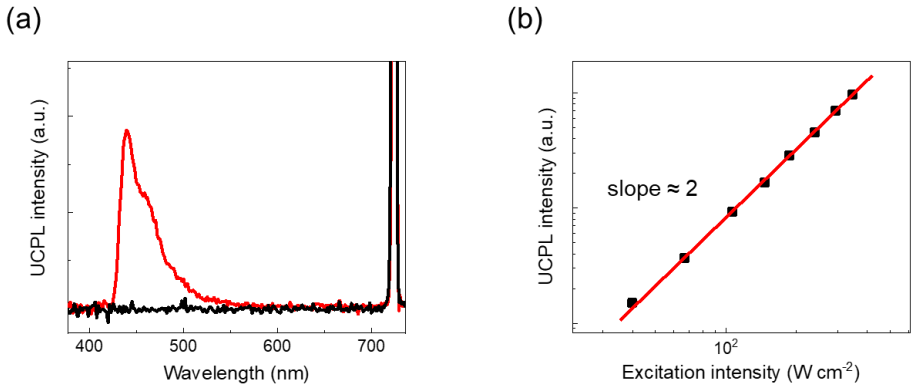

Figure 4-13. (a) Photoluminescence spectra of BPA in chloroform (100 mM) under deaerated condition (red, Ar atmosphere) and under aerated condition (black) upon excitation with a 724 nm laser at 145 W cm^{-2}. Scattered incident light and the residual phosphorescence were removed by short-pass filters (λ = 590 nm, λ = 690 nm). The measurements were performed at room temperature. (b) UC emission intensity for BPA in deaerated chloroform (100 mM) as a function of the excitation intensity (λ_{ex} = 724 nm). A red line shows the fitting result with slope of 2. The measurement was performed at room temperature under Ar atmosphere.

As demonstrated, the advantage of sensitizer-free TTA-UC is larger anti-Stokes shifts compared to those of the conventional TTA-UC systems. Meanwhile, large spin-orbit coupling reduces the fluorescence efficiency, which would naturally lead to the lower UC efficiencies. The estimation of UC efficiency in the sensitizer-free TTA-UC system was practically difficult because of the extremely small S-T absorption intensities to be quantified and the presence of light scattering that hampered its accurate estimation. The current sensitizer-free S-T absorption-based UC approach is considered to be complementary to the conventional two component TTA-UC systems and compensate for the shortcomings of conventional solid UC system, *i.e.*, energy losses intrinsic to the ISC of the sensitizers and the sensitizer-to-emitter TET.

4-2-2. Sensitizer-free TTA-UC properties of perylene derivatives

We generalized the S-T absorption-based TTA-UC in crystals of brominated emitters using another chromophore system. A new perylene derivative, 3-bromo-2,5,8,11-tetra-*tert*-butylperylene (BTBP) was synthesized by bromination of 2,5,8,11-tetra-*tert*-butylperylene (TBP). The T_1 energy level of perylene derivatives locates in the NIR region (~800 nm, 1.6 eV). TBP was employed as the parent molecule because the four bulky *tert*-butyl groups avoid the stacking of perylene core that causes large red shifts of fluorescence.[22, 23]

The crystal structure of BTBP was solved in this study (Figure 4-14a). As expected, the perylene core is isolated by the tethered *tert*-butyl groups, and bromine atoms are statically disordered in four positions. Interestingly, the perpendicular molecular alignment between two perylene chromophores forced the Br atom to be in close contact with the aromatic surface of next perylene core (Figure 4-14b), which would be advantageous for the intermolecular heavy atom effect. The phase purity of the crystal was confirmed by the good agreement between the experimental X-ray powder diffraction (XRPD) pattern and the simulation pattern obtained from the crystal structure (Figure 4-14c).

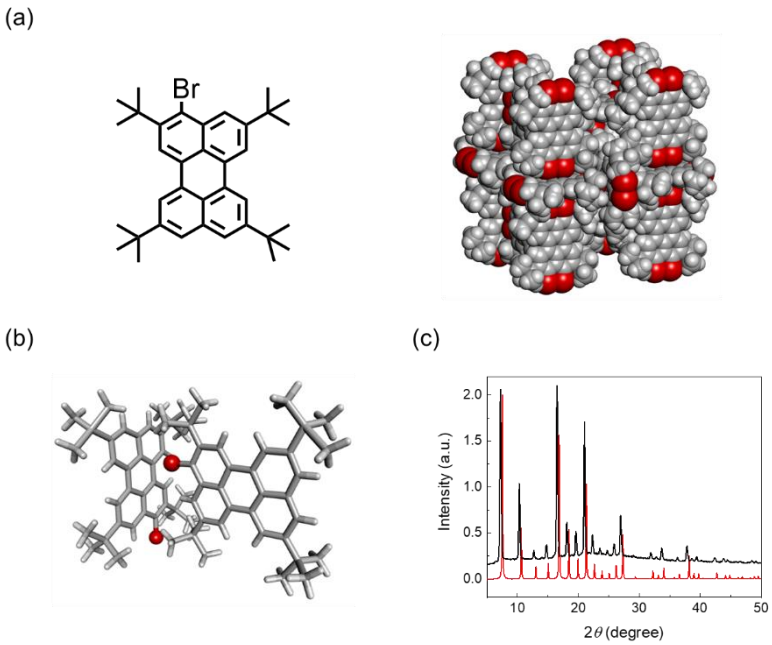

Figure 4-14. (a) Chemical and crystal structure of BTBP. Red, gray and white balls represent bromine, carbon and hydrogen atoms, respectively. (b) The nearest dimer of BTBP in the crystal structure. (c) XRPD pattern (black) of BTBP crystals together with the simulated pattern (red) obtained from the crystal structure.

Reflecting this unique perpendicular molecular alignment in crystals, the absorption and fluorescence spectra of BTBP showed much smaller red shifts as compared with those observed for stacked perylene chromophores (Figure 4-15).[24]

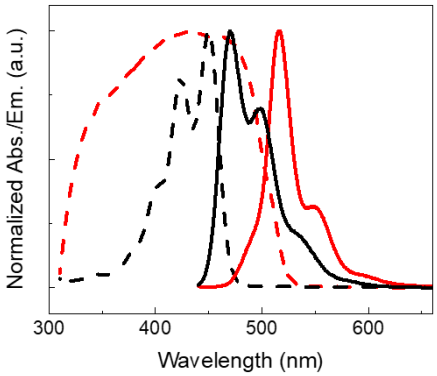

Figure 4-15. Normalized absorption (dashed lines) and fluorescence (solid lines) spectra of BTBP in chloroform (black, 10 μM) and in the solid state (red).

Significantly, the excitation of BTBP crystals by an 856 nm NIR laser produced UC emission at 520 nm (Figure 4-16a, red). There was no detectable UC emission from non-brominated TBP crystals (Figure 4-16a, black). As is the case in the brominated anthracene derivatives, BTBP had the quadratic excitation intensity dependence of UC emission intensity, which supports the TTA-based UC mechanism (Figure 4-16b). Thanks to the absence of energy losses by ISC and TET, a large anti-Stokes shift of 0.94 eV from NIR to green was achieved, demonstrating the generality and promising potential of S-T absorption-based strategy.

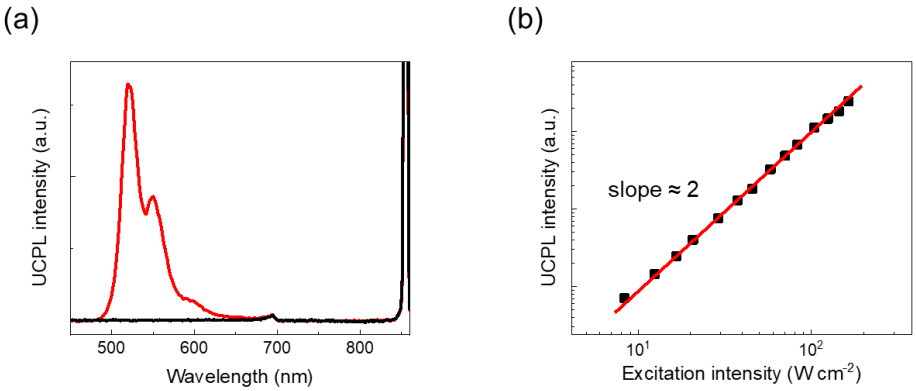

Figure 4-16. (a) Photoluminescence spectra of BTBP (red) and TBP (black) in the crystalline solid state upon excitation with an 856 nm laser at 135 W cm^{-2}. Scattered incident light and the residual phosphorescence were removed by short-pass filters (λ = 730 nm, λ = 840 nm). The measurements were performed at room temperature under Ar atmosphere. (b) UC emission intensity for crystalline BTBP as a function of the excitation intensity (λ_{ex} = 856 nm). A red line shows the fitting result with slope of 2. The measurement was performed at room temperature under Ar atmosphere.

4-3. Conclusion

In conclusion, sensitizer-free TTA-UC based on S-T absorption is demonstrated for single-component brominated organic crystals. This new approach simultaneously fulfills a large anti-Stokes shift and a relatively low excitation intensity, which is difficult to attain with conventional two-photon absorption (TPA) and sensitized TTA-UC mechanisms. The direct S-T absorption route circumvents the inevitable energy losses associated with the ISC and TET processes in sensitized TTA-UC, offering a powerful means to extend anti-Stokes shifts. In addition, the problem of inefficient sensitizer-to-emitter TET in binary crystals caused by segregation of these components is avoided in the current sensitizer-free UC system. It is to note that UC emission was clearly observable under excitation intensities in the order of ~W cm^{-2}, which is much lower than the TPA-based mechanism. Moreover, as another advantage over conventional sensitized UC system, this approach allows us to eliminate the use of precious heavy metals, which is favorable in terms of low cost and toxicity. Heavy atom effect for the enhanced S-T absorption inevitably causes the reduction of fluorescence efficiency, which may put restrictions to achieve a high UC efficiency. This issue, however, would be solved by exploration for chromophore assembly systems with the optimal balance between S-T absorption coefficient and fluorescence quantum yield.

The present system of NIR-to-visible upconversion will be applicable to water-dispersible nanocrystals, and a wide range of applications are envisaged including bioimaging, drug release and photodynamic therapy, which takes advantage of the high permeability of NIR light in living systems without causing cellular damage. Additionally, the finding obtained in this study provides a new perspective in the field of solid-state TTA-UC where simple halogenated organic compounds can be utilized as single-component UC materials. It would fertilize the chemistry and physics of luminescent organic materials.

4-4. Experimental

Materials

All reagents and solvents were used as received otherwise indicated. Anthracene was purchased from Sigma-Aldrich. 9-Bromoanthracene (BA, >95.0%), 9,10-dibromoanthracene (DBA, >98.0%), 9-bromo-10-phenylanthracene (BPA, >98.0%) and 2,5,8,11-tetra-*tert*-butylperylene (TBP, >97.0%) were purchased from TCI. Anthracene and all the brominated anthracene derivatives were purified by recrystallization in toluene before use.

Synthesis of 3-bromo-2,5,8,11-tetra-*tert*-butylperylene (BTBP)

To a DMF (40 mL) solution of TBP (255 mg, 0.53 mmol), DMF (10 mL) solution of *N*-bromosuccinimide (105 mg, 0.59 mmol) was slowly added, and the solution was stirred for 24 h at room temperature. H_2O (300 mL) was added to precipitate the products. The solid was collected by suction filtration. Column chromatography using *n*-hexane gave pure BTBP (bright yellow powder, 180 mg, 60%).

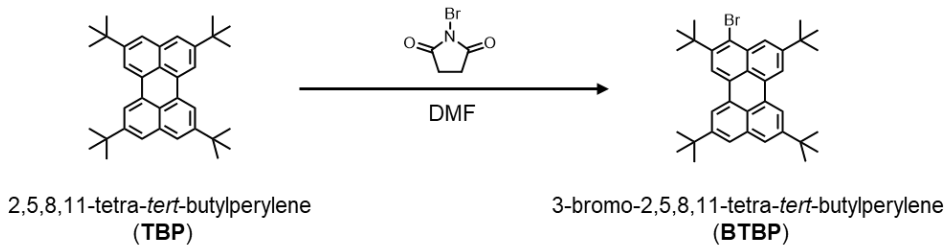

Figure 4-17. Scheme for the synthesis of BTBP.

^{1}H NMR (300 MHz, $CDCl_3$, TMS standard)

δ = 8.44-8.25 (m, 5H, Ar–H), 7.68 (s, 2H, Ar–H), 1.77 (s, 9H, CH_3), 1.55-1.5 ppm (m, 27H, CH_3).

Elemental analysis

Calculated (%) for $C_{36}H_{43}Br$: C 77.82, H 7.80. Found: C 77.81, H 7.81.

Sample preparation for TTA-UC measurements

The crystals of anthracene derivatives were sealed in glass cells of 1 cm thick in an Ar-filled glove box (oxygen concentration <0.1 ppm). The crystals of perylene derivatives were sandwiched between glass slides and sealed in the glove box. Chloroform solution of BPA was prepared in the glove box.

Characterization

Elemental analysis was conducted at the Elemental Analysis Center, Kyushu University. ^{1}H NMR (300 MHz) spectrum was measured on a Bruker DRX-spectrometer using TMS as the internal standard. X-ray powder diffraction (XRPD) analysis was conducted on a BRUKER D2 PHASER with a Cu Kα source (λ = 1.5418 Å). Single-crystal X-ray data were collected on a CCD diffractometer (Rigaku Saturn VariMax) with graphite-monochromated Mo Kα radiation (λ = 0.71070 Å). UV-vis absorption spectra were recorded on a JASCO V-670 or JASCO V-770 spectrophotometer. Transmission and diffuse reflection methods were employed for solution and solid samples, respectively. Fluorescence spectra were measured by using a PerkinElmer LS55 fluorescence spectrometer with a 1 mm path length cell. The samples were excited at an incidence angel of 45° to the quartz cell surface, and the fluorescence was detected along the normal. Time-resolved photoluminescence lifetime measurements were carried out by using a time-correlated single photon counting lifetime spectroscopy system, HAMAMATSU Quantaurus-Tau C11567-01.

For TTA-UC measurements, diode lasers (532 nm, 635 nm, 724 nm, 856 nm, RGB Photonics) were used as excitation sources. The laser power was controlled by combining a software (Ltune) and a variable neutral density filter, and measured using a PD300-UV photodiode sensor (OPHIR Photonics). The laser beam was focused on a sample using a lens. The diameter of the laser beam ($1/e^2$) was measured at the sample position using a CCD beam profiler SP620 (OPHIR Photonics). Accordingly, in our current setup, the maximum laser intensities for each laser are estimated as 740 W cm^{-2} (532 nm), 54.6 W cm^{-2} (635 nm), 389 W cm^{-2} (724 nm) and 135 W cm^{-2} (856 nm) at the sample position. The emitted light was collimated by an achromatic lens, the excitation light was removed using short-pass filters, and the emitted light was again focused by an achromatic lens to an optical fiber connected to a multichannel detector MCPD-9800 (Otsuka Electronics).

References

[1] S. Baluschev, V. Yakutkin, G. Wegner, B. Minch, T. Miteva, G. Nelles, A. Yasuda, *J. Appl. Phys.* **2007**, *101*, 023101.

[2] P. Duan, N. Yanai, N. Kimizuka, *J. Am. Chem. Soc.* **2013**, *135*, 19056-19059.

[3] R. Vadrucci, C. Weder, Y. C. Simon, *J. Mater. Chem. C* **2014**, *2*, 2837-2841.

[4] O. V. Mikhnenko, P. W. M. Blom, T.-Q. Nguyen, *Energy Environ. Sci.* **2015**, *8*, 1867-1888.

[5] N. Yanai, N. Kimizuka, *Chem. Commun.* **2016**, *52*, 5354-5370.

[6] H. Kouno, T. Ogawa, S. Amemori, P. Mahato, N. Yanai, N. Kimizuka, *Chem. Sci.* **2016**, *7*, 5224-5229.

[7] N. Kimizuka, N. Yanai, M. Morikawa, *Langmuir* **2016**, *32*, 12304-12322.

[8] J. Trotter, *Acta Crystallogr C* **1986**, *42*, 862-864.

[9] CCDC 1530375 (BPA) and 1530376 (BTBP) contain the supplementary crystallographic data for this paper. These data can be obtained free of charge from The Cambridge Crystallographic Data Centre via www.ccdc.cam.ac.uk/data_request/cif.

[10] M. Montalti, A. Credi, L. Prodi, M. T. Gandolfi, *Handbook of photochemistry, third edition*, CRC Press, Boca Raton, **2006**.

[11] G. F. Moore, I. H. Munro, *Nature* **1965**, *208*, 772-773.

[12] S. Baluschev, V. Yakutkin, T. Miteva, G. Wegner, T. Roberts, G. Nelles, A. Yasuda, S. Chernov, S. Aleshchenkov, A. Cheprakov, *New J. Phys.* **2008**, *10*, 013007.

[13] M. Pope, C. E. Swenberg, *Electronic processes in organic crystals and polymers*, Oxford University Press, New York, **1999**.

[14] G. D. Gillispie, E. C. Lim, *J. Phys. Chem.* **1976**, *65*, 2022-2023.

[15] A. Monguzzi, J. Mezyk, F. Scotognella, R. Tubino, F. Meinardi, *Phys. Rev. B* **2008**, *78*, 195112.

[16] T. W. Schmidt, F. N. Castellano, *J. Phys. Chem. Lett.* **2014**, *5*, 4062-4072.

[17] O. Bolton, K. Lee, H.-J. Kim, K. Y. Lin, J. Kim, *Nat. Chem.* **2011**, *3*, 205-210.

[18] Z. An, C. Zheng, Y. Tao, R. Chen, H. Shi, T. Chen, Z. Wang, H. Li, R. Deng, X. Liu, W. Huang, *Nat. Mater.* **2015**, *14*, 685-690.

[19] S. Mukherjee, P. Thilagar, *Chem. Commun.* **2015**, *51*, 10988-11003.

[20] Y. Gong, L. Zhao, Q. Peng, D. Fan, W. Z. Yuan, Y. Zhang, B. Z. Tang, *Chem. Sci.* **2015**, *6*, 4438-4444.

[21] A. Sakai, E. Ohta, Y. Matsui, S. Tsuzuki, H. Ikeda, *ChemPhysChem* **2016**, *17*, 4033-4036.

[22] R. O. Al-Kaysi, T. Sang Ahn, A. M. Müller, C. J. Bardeen, *Phys. Chem. Chem. Phys.* **2006**, *8*, 3453-3459.

[23] X. Zhang, C. Dong, J. A. Zapien, S. Ismathullakhan, Z. Kang, J. Jie, X. Zhang, J. C. Chang, C.-S. Lee, S.-T. Lee, *Angew. Chem. Int. Ed.* **2009**, *48*, 9121-9123.

[24] J. Tanaka, *Bull. Chem. Soc. Jpn.* **1963**, *36*, 1237-1249.

Chapter 5. Conclusion

In this thesis, three types of TTA-UC systems were proposed to solve the intrinsic problem in conventional system sensitized by molecular sensitizer: the limitation of anti-Stokes shifts due to energy losses during the triplet sensitization process.

In Chapter 2, CdSe/ZnS core-shell quantum dots (QDs) were used as triplet sensitizers in substitution for common organic sensitizers. The QD-based mechanism includes no significant energy loss in intersystem crossing process of sensitizers, which has potential to realize larger anti-Stokes shifts. In fact, a large anti-Stokes of 0.91 eV was achieved in both solution and solid state. The surface modification of core-shell QDs with energy transmitter molecules played a key role in the efficient energy transfer to emitter molecules in bulk solution. Interestingly, UC properties were improved with CdSe/ZnS core-shell QDs compared to CdSe core-only QDs, which should be derived from the reduced surface traps on core-shell QDs. By taking advantages of QDs such as their broadband absorption and tunable bandgaps, the QD-based TTA-UC is highly expected as spectrally versatile system. Together with the findings obtained by this work and others, this system will become a powerful mean for the efficient NIR-to-visible UC.

In Chapter 3, $CsPb(Cl/Br)_3$ perovskite nanocrystals (PNCs) were used as another type of inorganic triplet sensitizer. The first example of visible-to-UV TTA-UC sensitized by PNCs was demonstrated, in which the anti-Stokes shift reached 0.88 eV at maximum. As is the case with the triplet sensitization by QDs, efficient triplet sensitization was possible only in the presence of transmitter molecules. The control experiments clarified that an appropriate triplet energy level and its binding to PNC surface are essential for transmitters to mediate triplet energy transfer. This work proved the high triplet sensitization capability of transmitter-modified PNCs. By investigating new transmitter ligands or other perovskite families, more efficient TTA-UC system with a desired spectral range will be accomplished.

In Chapter 4, S-T absorption-based sensitizer-free UC system was demonstrated, where energy losses in triplet sensitization process are eliminated. Although S-T absorption is spin-forbidden, modification of chromophores with bromine allowed the direct population of excited triplets at excitaton intensities of ~W cm^{-2}. The subsequent triplet energy migration and TTA events in crystals of brominated anthracene derivatives lead to upconversion of NIR light to blue light, in which the maximum anti-Stokes shift was 0.96 eV. The generality of this strategy was confirmed for crystals of a brominated perylene derivative that showed green UC emission under longer wavelength NIR excitation. Whereas further development is needed, this approach offers a clue for the future design of TTA-UC system.

Finally, TTA-UC systems in the studies described are summarized in Figure 5-1.

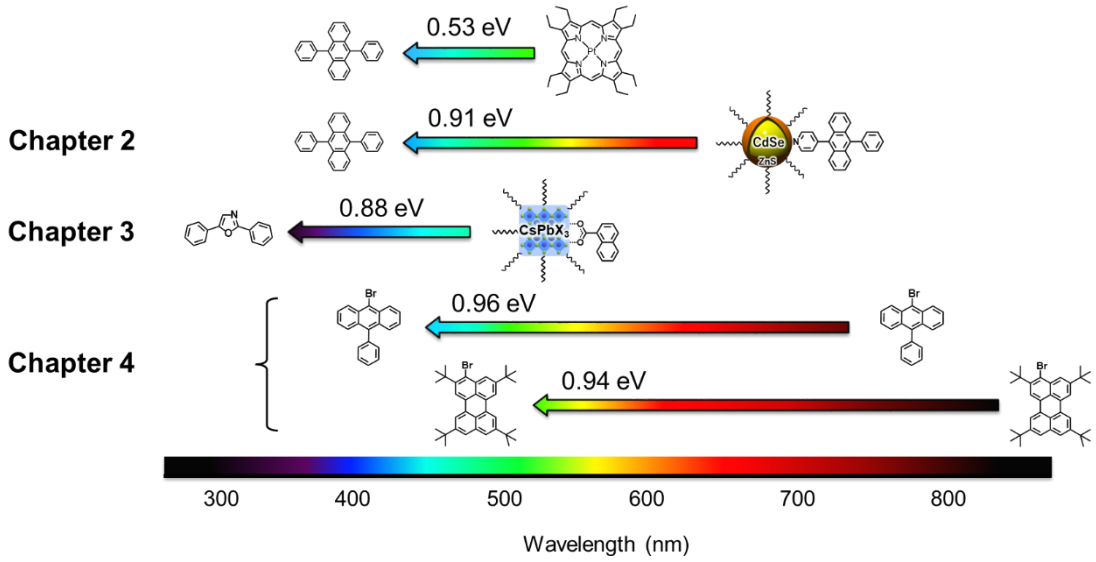

Figure 5-1. Overview of the TTA-UC systems in the studies described, along with a benchmark system of platinum (II) octaethylporphyrin (PtOEP, sensitizer) and 9,10-diphenylanthracene (DPA, emitter).

Acknowledgments

The study in this thesis has been carried out under the direction of Professor Nobuo Kimizuka during April 2015 – March 2020 at the Department of Chemistry and Biochemistry, Graduate School of Engineering, Kyushu University.

I would like to express my sincerest gratitude to Professor Nobuo Kimizuka for guiding me with valuable suggestions and warm encouragement. I wish to extend my heartfelt appreciation to Associate Professor Nobuhiro Yanai for his helpful suggestions, fruitful discussions and persistent help. I deeply grateful to Associate Professor Teppei Yamada, Associate Professor Shigenori Fujikawa, Assistant Professor Masa-aki Morikawa and Assistant Professor Joseph Ka Ho Hui for their precious advice and meaningful discussions. I am indebted to the technical staffs in this laboratory, Ms. Kazumi Matsuno, Ms. Azusa Suematsu, Ms. Chihoko Fukakusa and Ms. Ryo Maeda for their generous supports and encouragement. I sincerely appreciate Professor Satoru Kidoaki and Professor Noriho Kamiya for reviewing this thesis.

I wish to express my gratitude to Professor Pengfei Duan (National Center for Nanoscience and Technology, China), Assistant Professor Shogo Amemori (Kanazawa University), Dr. Kouta Masutani, Dr. Deepak Asthana, Dr. Rakesh Kumar Gupta, Dr. Pankaj Bharmoria, Dr. Biplab Joarder, Dr. Tejwant Singh, Dr. Arijit Mallick, Dr. Gurbir Singh, Dr. Keita Ishiba, Dr. Taku Ogawa, Dr. Kazuma Mase, Dr. Hisanori Nagatomi, Dr. Masaya Matsuki, Dr. Shota Hisamitsu, Dr. Masanori Hosoyamada, Mr. Taro Wakiyama, Ms. Rina Yoshida, Dr. Yimin Liang, Mr. Tsubasa Kashino, Mr. Hironori Kouno, Mr. Kanji Shiraishi, Mr. Ryosuke Yamamoto, Mr. Keisuke Kanakogi, Mr. Yuta Kubo, Mr. Tomoya Shimono, Ms. Mariko Kozue, Mr. Shinya Uchino, Mr. Hirotaka Ohara, Mr. Yoichi Sasaki, Ms. Hanyu Yang, Mr. Toshiki Eguchi, Mr. Hongyou Zhou, Mr. Yuki Nagai, Ms. Nao Hirakawa, Mr. Saiya Fujiwara, Mr. Junji Miyano, Ms. Xiaopeng Zou, Mr. Yusuke Kawashima, Mr. Zheng Yan, Ms. Risa Okeda, Ms. Mika Kinoshita, Mr. Takashi Kobayashi, Mr. Tetsuro Kobayashi, Mr. Keisuke Hayashi, Ms. Rena Haruki, Mr. Koki Nishimura, Ms. Fan Gao, Mr. Hirotaka Inoue, Ms. Risa Iwami, Ms. Kana Orihashi, Mr. Kwak Donggyu, Ms. Mio Koharagi, Ms. Mone Sakata, Mr. Yuichiro Seki, Mr. Naoyuki Harada, Mr. Issei Maruyama, Ms. Kanae Izumi, Mr. Junpei Kondo, Mr. Kentaro Tanaka, Mr. Ryoichi Tomomatsu, Mr. Tomoyuki Hamachi, Mr. Fumitoshi Matoba, Mr. Akio Yamauchi and Ms. Naura Fakhira Antariksa for warm supports and constructive discussions. I am grateful to the support by JSPS KAKENHI Grant Number JP17J04798.

Finally, I would like to extend my special thanks to my family for their enormous supports and encouragement.

Keisuke Okumura

Department of Chemistry and Biochemistry

Graduate School of Engineering, Kyushu University

March 2020